

# Kennisagenda Aardwarmte

First estimate on the potential of soft simulation by means of acid and hydraulic treatment technics in the Triassic sandstone for geothermal heat and power provision.

November, 2016



Authors: Anna Peksa  
Naveen Ilangovan  
Fiorenza Deon  
Hamidreza M. Nick  
David Bruhn



Ministerie van Economische Zaken



Table of contents

<b>1</b>	<b>INTRODUCTION.....</b>	<b>3</b>
<b>2</b>	<b>MODELING APPROACH .....</b>	<b>5</b>
2.1	PHYSICAL PHENOMENA.....	5
2.2	CORE SCALE MODEL.....	5
2.3	FIELD SCALE MODEL .....	5
<b>3</b>	<b>EXPERIMENTAL APPROACH.....</b>	<b>5</b>
3.1	MATERIALS .....	5
<b>4</b>	<b>NUMERICAL MODEL RESULTS .....</b>	<b>21</b>
4.1	CORE SCALE MODEL.....	21
4.2	HOMOGENEOUS SYSTEM .....	23
4.3	HETEROGENEOUS MODEL .....	27
<b>5</b>	<b>EXPERIMENTAL RESULTS.....</b>	<b>29</b>
5.1	ACID INJECTION INTO INTACT ROCK .....	29
5.2	ACID INJECTION INTO FRACTURED ROCK WITH A CONTROL OVER THE CONFINING PRESSURE.....	29
<b>6</b>	<b>CONCLUSIONS .....</b>	<b>35</b>
<b>7</b>	<b>ACKNOWLEDGMENTS.....</b>	<b>36</b>

## 1 Introduction

With increasing share of geothermal energy within the Dutch energy market, the project aims to help in reducing the consumption of fossil fuels and CO<sub>2</sub> emission. Depending on the depth of the wells, geothermal projects can produce heat and electricity, reducing gas and electricity use respectively. The Dutch geothermal resources are extensive and can provide a base to both increase energy production and make energy production more sustainable. The project contribute in making geothermal energy provision more attractive for the energy market by increasing the control on the stimulation treatment and reducing required times and costs, even in low enthalpy geothermal reservoirs. Thereby, this project contributes to solve the global energy problem.

The target reservoir is located in the Westland area in the Netherlands and belongs to the sandstone Triassic formations that are considered as potential geothermal reservoirs. In these formations the permeability of the rock matrix can be very low for geothermal energy production and fractures may become the main pathways for flow. Formations having an average effective permeability of 1-10 mD or less generally requires stimulations techniques to improve injectivity/productivity.

To enlarge the pore spaces for fluid flow in the sandstones, a matrix acidizing can be used by dissolving the pore lining materials (like clays, carbonates) that are more vulnerable to acid attack than any framework minerals. However, the availability of the pore lining minerals and their surface area are the key factors that contribute to an efficient and successful matrix dissolution by injected acids. In the target Hardeggen reservoir, the preliminary studies conducted by TNO and T&A suggested carbonates as main objectives to acid stimulation. However, after conducting detailed mineralogical analyses of the samples from Volpierhausen formation, acidizing is recommended to be (as well) directed to dissolving minerals, such as, clays that may adversely affect the permeability of the system when exposed to injection and drilling fluids.

The formation may contain natural fractures that can be the most probable flow path from the injection to the production well. In relation to this, if the wells are drilled through the fracture zones, it might be possible to encounter various formation damage problems and that fractures can become clogged. In both cases, acid treatment can be applied in the porous system for either conductivity improvement of the natural fractures, or for damage removal.

The aquifer proposed for thermal extraction, is situated in the heterogeneous West Netherlands Basin (WNB) and includes the geothermal licenses Naaldwijk en Maasland where wells will be drilled to the depth of 4 km. Special care needs to be taken in the planning and designing of the acid injection in order to prevent any possible formation damage. One has to keep in mind that at high depths, temperatures and pressures are in the higher ranges where stability of certain minerals in contact with reactive agent is disturbed. As well injection pressures during acid works may exceed the static wellhead pressure due to high pressure drops.

In this study a series of laboratory core-flooding experiments were conducted to investigate the potential for matrix acidizing in the prospective geothermal reservoirs. The experimental part comprises of the injection of an acidizing agent into cylindrical heterogeneous Middle Buntsandstein cores (both with and without fractures) after bine

## kennisagenda Aardwarmte: Soft stimulation techniques - D2

injection to mimic reservoir conditions. The Computed Tomography (CT) technique is used to support tests on the fractured rocks and to visualize fracture aperture changes while flow tests are conducted.

The objective of this study is twofold: (1) to investigate the effect of injected fluids on the intact rocks in the near-wellbore area; (2) to quantify changes in permeability in the fractured rocks as a preliminary study to design optimal conditions for matrix acidizing in sandstone type reservoirs. By this it is a contribution to achieve an increase in renewable energy production in heterogeneous, deep geothermal environments.

This study is a continuation of TNO studies where only dissolution tests were conducted over the investigated samples.

## **2 Modeling approach**

Core scale and field scale 3-Dimensional finite element models were created for the purpose of this study.

### **2.1 Physical phenomena**

The following physical phenomena are considered in the finite element coupled reactive flow model: (1) transport of chelating agent and/or other fluids in the reservoir; (2) fluid/rock interaction resulting in permeability and porosity alteration; (3) Heat transfer in the subsurface for geothermal extraction.

### **2.2 Core scale model**

In the case of the core scale model, the model is matched with the results from the experiments. All the conditions that were used in the experiment are accounted for in the model. Darcy's law for porous media and transport of diluted species in porous media were used for modelling the transport and the rock-fluid interactions respectively. The dissolution of carbonates is implemented by using a domain scale ordinary differential equation. The main uncertain parameter is the surface area available for fluid-rock interaction which is varied to match the experimental data.

### **2.3 Field scale model**

Two studies were conducted in this model for studying the effect of calcite dissolution in the field scale. Similar to Crooijmans et al., (2016) a heterogeneous reservoir with an injection and production well was built for this part of the study. For computational and ease of modelling, the fracture network is not considered but an average initial permeability is considered. As mentioned earlier, this model uses the parameters obtained from the core scale model and studies the effect of well stimulation in field scale. The same physics that were used in the core scale model are used in this model as well. The second field scale study imports the altered permeability and porosity distribution from the previous field scale model and is used to study the effect on the energy production. Darcy's law and heat transfer in porous media were the physics used to model the flow of mass and heat respectively.

#### **2.3.1 Boundary and initial conditions – field scale model**

The boundaries on the sides of the reservoir were assigned constant pressure boundary condition. The top and bottom boundaries were assumed to be a sealing layer with no heat loss. A constant initial reservoir temperature and pressure were determined based on the geothermal and hydrostatic pressure gradient which is a function of the reservoir depth. Similar to Crooijmans et al., (2016) and Saeid et al., (2015), the density, viscosity and thermal conductivity of water, fluid (acid)-rock reaction rate are established as a function of temperature respectively.

## **3 Experimental approach**

### **3.1 Materials**

Acid flooding experiments were conducted on the heterogeneous samples from the Triassic formation that were obtained from the reservoirs and on their quarry analogs. In this section of the study the used samples together with their mineralogical composition and the used fluids are described.

### 3.1.1 Samples

#### 3.1.1.1 Samples origin - regional geology

The aquifer proposed for thermal extraction, is situated in the West Netherlands Basin (WNB) and includes the geothermal licenses Naaldwijk en Maasland (see Fig. 3.1). It spans the whole Main Buntsandstein (lower Germanic Trias), and thus contains lithostratigraphic members from the Volpriehausen, the Detfurth and the Hardegsen Formation. Table 1 shows the corresponding stratigraphic framework of the Triassic in the Netherlands. In the following, the Main Buntsandstein subgroup in the West Netherlands Basin which consists of the three previously mentioned, fining upward formations is shortly described. For more details about the depositional environment and geology, the reader is referred to previous analyses of cores, wireline logs, outcrops and analogues from the same formations carried out by TU Delft (e.g. Matev 2011; Ogunjimi 2010) and by industry partners (Brugge et al., 2013).

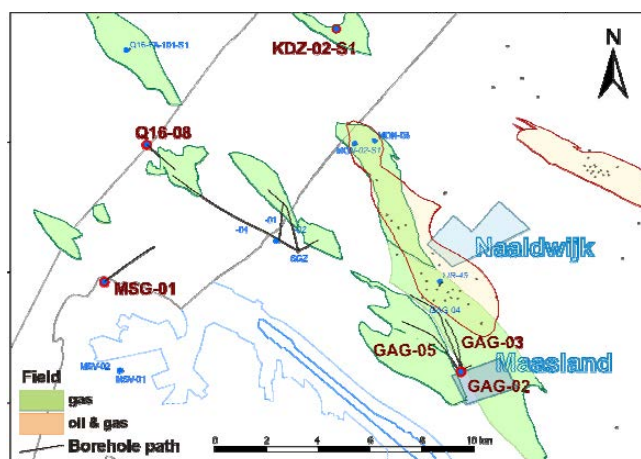


**Fig. 3.1** Study areas of geothermal licences Naaldwijk and Maasland, and locations of nearby wells previously used for petrophysical analysis of the Triassic reservoirs (blue and red dots) (after T&A rapport).

**Volpriehausen Formation.** The Volpriehausen formation are a stacked sequence of cross and parallel cross bedded sandstones with abundance of mud clasts. It's grain size varies from fine to medium grained with occasional silt laminations. The sandstones are arkosic with a quartz content slightly below 50% and are cemented by high percentages of calcite and dolomite, especially in its lower part.

**Detfurth Formation.** In areas where the formations is well developed, the Lower Detfurth consists of clean sand intervals of several meters. Towards the Upper Detfurth the formation becomes a mixture of various depositional environments with a gradually increasing amount of aeolian sediments. It's grain sizes ranging from clay and silt to fine sand and occasional medium sand aeolian layers are usually poor sorted (with exception of dune sands) and it's quartz content and cementation varies. In the West Netherlands Basin the formation consists entirely of sandstones and the depositional thickness of the formation is about 20-40 m. It serves as the connection between the fluvial dominated Volpriehausen and more aeolian/desert environment dominated Hardegsen formation.

**Hardegens formation.** The Hardegens formation represents a shift towards a clearly defined desert setting with aeolian dunes and damp sand flats and consists predominantly of siltstones, with subordinate, thin sandstone beds (Matev 2011). Further, the Hardegens formation is characterized by poor matrix permeability and flow is mainly controlled by natural fracture and faults network. In the West Netherlands Basin its thickness reaches up to 70 m (see Fig. 3.2).

**Table 1** Stratigraphy of the Triassic in the Netherlands (after Matev 2011).

	Formation	Lithology	Thickness [m]	Depth range [m]
<b>Upper Germanic Trias</b>	Sleen	Grey shales & brown limestone	45	40-4450
	Keuper	Evaporites & Claystones	>1000	850-3900
	Muschelkalk	Limestone & Evaporites	500	outcrop-3950
	Roet	Evaporites, clay- & Siltstone	300	outcrop-4200
	Solling	Sand- & Clay stone	125	90-4250
<b>Lower Germanic Trias</b>	Hardegens	Sand- & Clay stone	200	680-4350
	Detfurth	Sand- & Clay stone	100	270-4500
	Volpriehausen	Sand- & Clay stone	200	125-4750
	Lower Bunsandstein	Varicoloured sand&claystone	400	80-5000

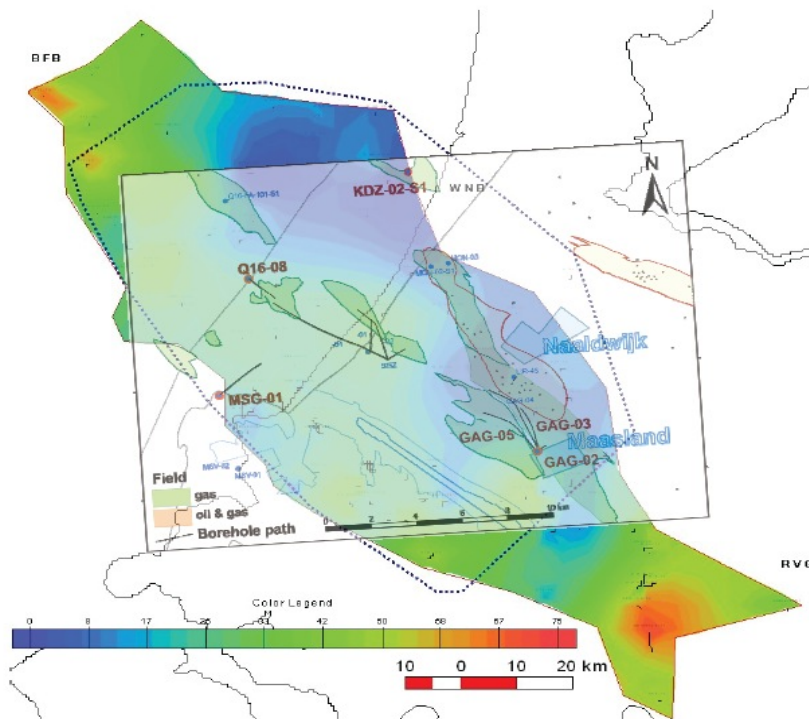


**Fig. 3.2** Basic thickness map of Hardegens formation overlain by study area (after Matev 2011).

### 3.1.1.2 Sample characterization

Routine core displacement tests were carried out on sandstone cores from the above described Main Buntsandstein formation. The main experimental material was collected from existing boreholes, however, additional material needed to be obtained from outcrop locations. Due to limited availability of the Hardegsen Formation samples, the investigation of the well samples for final tests was diversified throughout the Main Buntsandstein (MB) formation (Fig. 3.3). The sedimentary facies in the larger interval are exhibiting similarities. Selection of the appropriate samples was done based on available mineralogical/petrographic composition data in the literature and the geological conditions determined from the well cores in the Westland concession. The selection of samples was directed towards low porosity sandstones, as according to Nelskamp and Verwey (2012), the average reservoir porosity of the Triassic Formation at 4 km depth may not exceed 8% and permeability may be around 4 mD.

In this regard, analog sandstones (both well and outcrop) with similar properties and cement types – regardless of their stratigraphic position were chosen (Table 2); three different outcrop samples from Germany and one offshore sample from a borehole Q16-02 from depths of 3629 – 3838 m (Fig. 3.3). It should be noted that in this project, a material not characterized previously was studied. The well bore samples that are used in this study were assumed in the TNO report as similar to the Detfurth formation. Further discussion on this point can be found in section 3.1.1.3. A summary of collected borehole samples is presented in appendix 1.

**Table 2** Representative selected rock samples from the Lower Germanic Triassic Group.

Name of the rock	name	Location	Stratigraphy
<b>Borehole</b>	Q16-02	Offshore	MB, Volpriehausen
<b>Wesersandstein (Quarry)</b>	W-1	Bad Karlshafen, North Hessen	MB, Solling-Folge, Karlshafener Schichten
<b>Friedewalder Buntsandstein, pale. (Quarry)</b>	F-1	Friedewald, South Hessen	MB, Solling-Folge
<b>Kordeler Sandstein (Quarry)</b>	K-1	Trier, Rhineland-Palatinate	Upper Buntsandstein Vltziensandstein

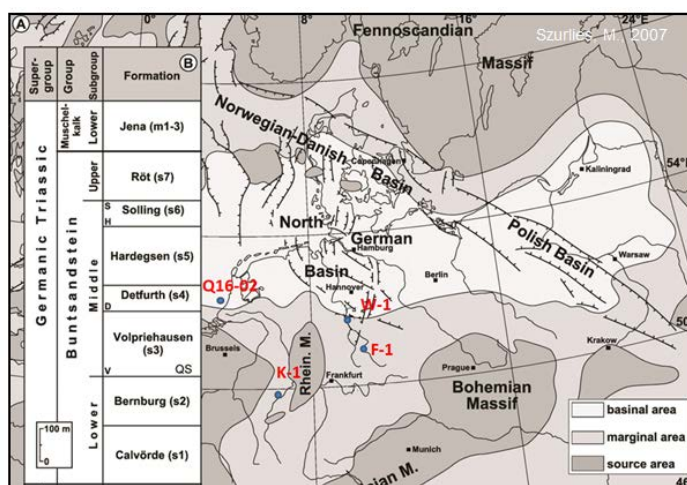


**Fig. 3.3** Locations of the selected samples.

### **3.1.1.3 Petrophysical characterization of the samples**

To improve the success of sandstone-acidizing, the mineral composition of the target formations must be known in detail. Otherwise, problems with clay swelling, fines migration, gel formation, and precipitation can be encountered. Moreover, the mineral composition is necessary for proper injection acid determination.

The combination of following methods: XRD powder diffraction, XRF, microscope analysis, scanning electron microscope (SEM) and electron Microprobe (EMP) provides a complete description and interpretation of the rock. Moreover, the rock properties such as porosity and permeability were measured with use of Ultrapycnometer 1000, calculated from CT-scans and measured during flow experiments respectively.

#### **Electron-microprobe analysis (EMPA)**

Single-spot mineral analyses were performed using a CAMECA SX100 electron microprobe operating in the wavelength-dispersive mode at the Electron Microprobe Laboratory, Department of Inorganic and Isotope Geochemistry at the Helmholtz Centre Potsdam – German Research Centre for Geosciences (GFZ) in Potsdam, Germany. The analytical conditions include an accelerating voltage of 15 kV, a beam current of 10 nA, and a focused beam. Well-characterized grains of plagioclase and quartz were used as standards. Secondary-electron (SE) images were collected with a JEOL JXA 8230 electron microprobe (15 kV accelerating voltage) in the same laboratory.

#### **X-Ray diffraction analysis (XRD)**

*The following procedure has been taken from Deon et al. (2015). The instruments used for this study are located at TUD. However, the measurement procedure and scope of the analyses is very similar to the procedures adopted in Deon et al. (2015).*

To determine the modal mineralogy of the rocks by XRD, the rock samples were crushed and sieved to obtain the 63- $\mu\text{m}$  fraction. XRD patterns were recorded in transmission using a fully automated STOE STADI P diffractometer (Cu-K $\alpha$  radiation), equipped with a primary monochromator and a 7 $^\circ$ -wide position sensitive detector, at the Department of Chemistry and Physics of Earth Materials at GFZ. Semi-quantitative interpretation of the pattern has been carried out using EVA diffraction suite from Bruker. The diffractograms were refined with the EXPGUI-GSAS software (Larson and Von Dreele, 2000; Toby, 2001; Belsky et al., 2002), using reference structures from the ICDS database (Bergerhoff and Brown, 1987).

#### **Results for the mineral composition on sample W1 and Q16-02**

##### **Sample W1**

**Optical microscope images.** The optical observation at the microscope evidences a high concentration of quartz (Fig. 3.4a), microcline (Fig. 3.4b) and micas (Fig. 3.4c and d). The exact type of phyllosilicate could not be determined at the microscope. Grains with a size  $\geq 100 \mu$  characterize the sample (Fig. 3.4a). Quartz occurs with different extinction. Microcline can be recognized by the typical twinning which appears scattered in the thin section. Alteration has been detected throughout W1. However, the clay fraction cannot be recognized at the microscope. The sample has been investigated additionally by means of XRD and EMPA.

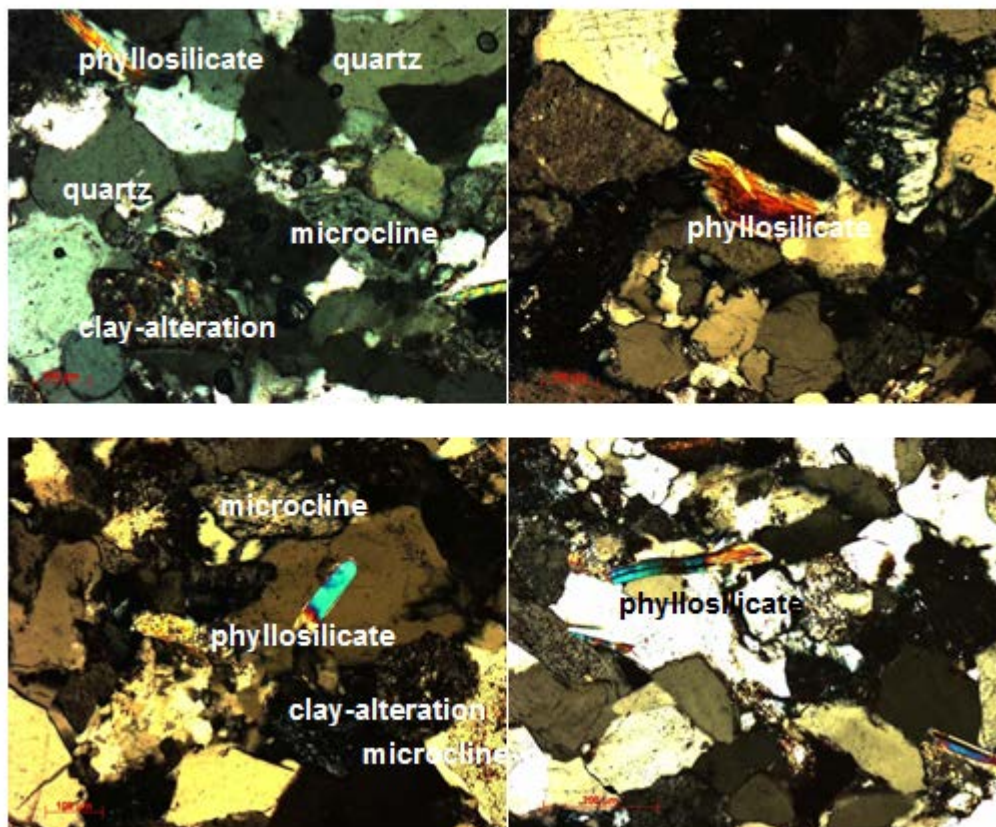


**Fig. 3.4** Optical representation of quartz which is the dominant phase occurring in the sample along with microcline, phyllosilicate and clay

### Electron microprobe (EMP)

In order to determine the chemical composition of each single crystal, well-polished thin sections of the W1 sample have been observed and analysed at the electron microprobe. An advantage of using the electron microprobe is the detection of mineral phases whose concentration lies below 1wt. %. Such minerals, like rutile and zircon in our case, could not be detected by XRD. The following secondary electron (SE) images have been collected at the Electron Microprobe at GFZ Potsdam. The images below represent a selection from many more acquired on the sample. We have opted for those relevant to evidence the presence of phyllosilicate and clay, which relevant mineral phases playing an important role in the outcome of this study. Fig. 3.5 offers an overview of the thin section where quartz, microcline, clay fraction and zircon can be observed. The most abundant phase in the sample is quartz followed by microcline, clay, phyllosilicate (mica or chlorite) and accessories (zircon and spinel). Fig. 3.6 presents the evidence of chlorite along with zircon and microcline. In Fig. 3.7 we can observe the typical occurrence of the clay fraction in this sample. Usually clay forms replacing microcline (or plagioclase or K-feldspar) when alteration processes take places. Fig. 3.7 and Fig. 3.8 show an additional microcline grain with quartz in the background. Interesting are the typical stripes of the microcline cleavage which allow to distinguish microcline from plagioclase and K-feldspar. Fig. 3.9 offers a nice view on the phyllosilicates occurring in this sample.

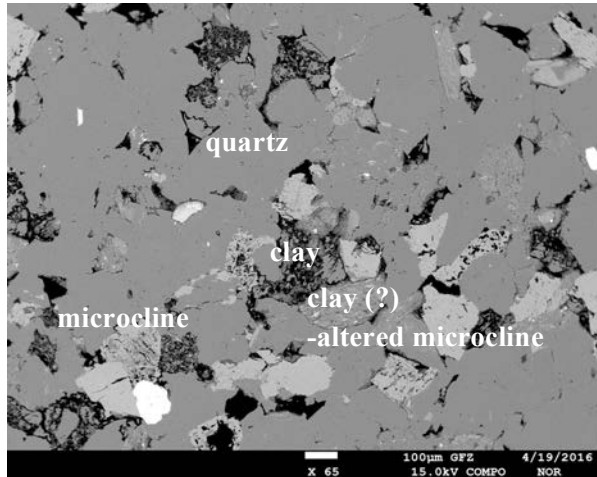


Fig. 3.5 Secondary electron image (W-1)

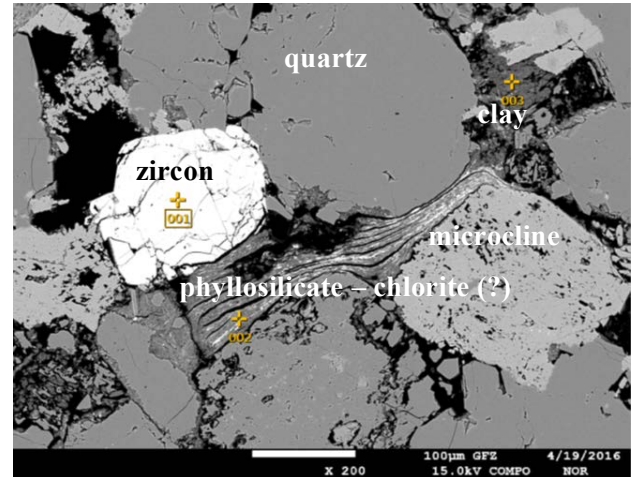


Fig. 3.6 Secondary electron image (W-1)

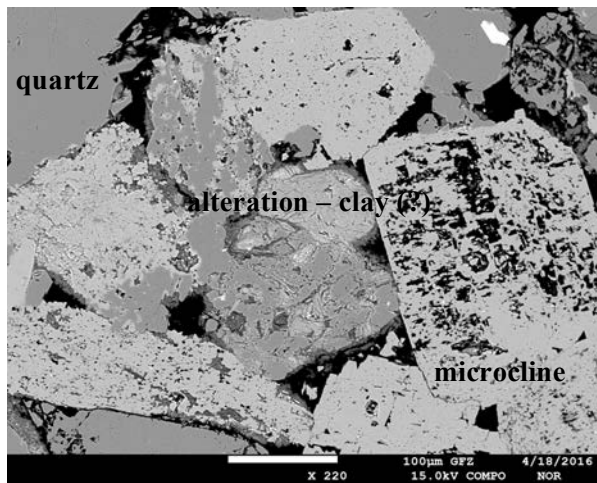


Fig. 3.7 Secondary electron image (W-1)

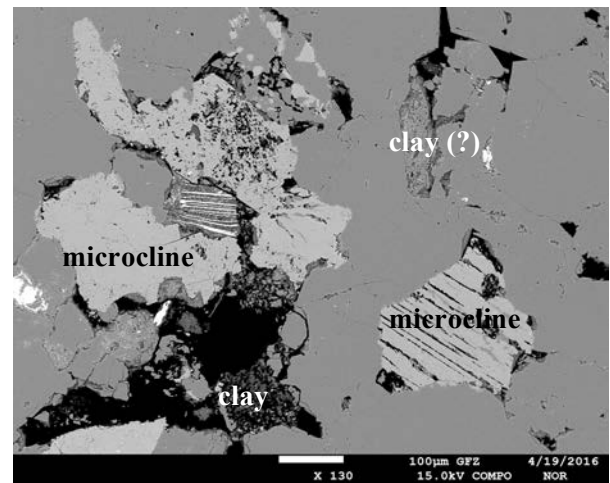


Fig. 3.8 Secondary electron image (W-1)

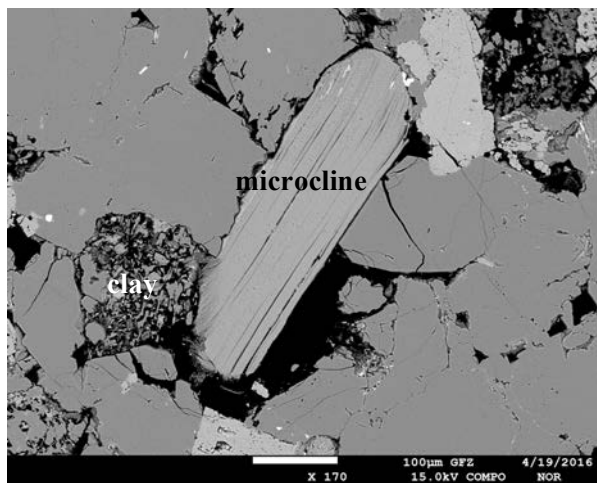
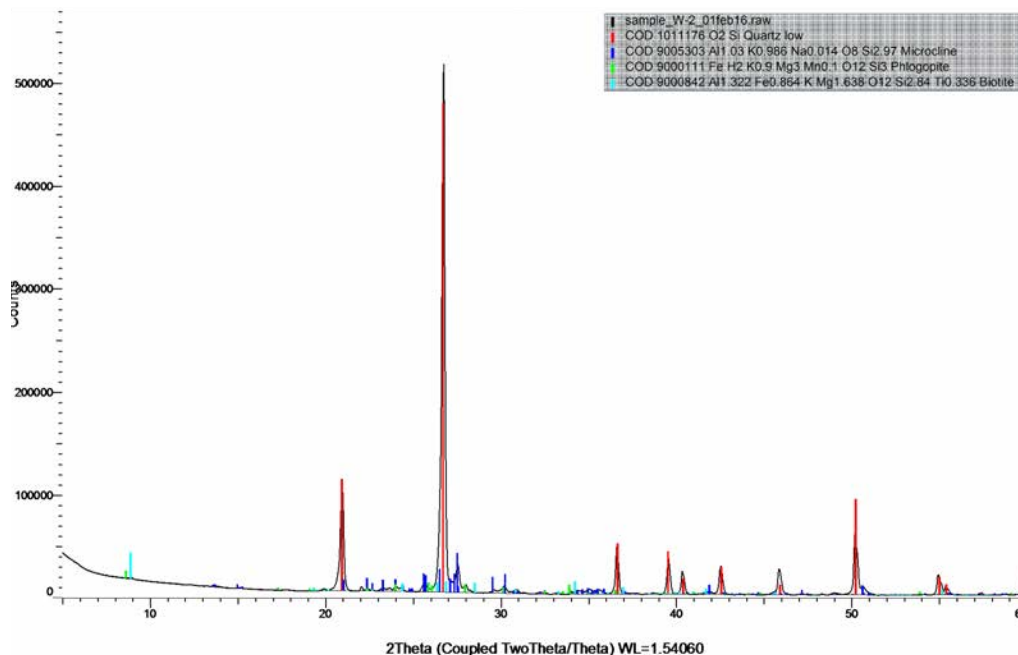


Fig. 3.9 Secondary electron image (W-1)

XRD. The XRD pattern shows major quartz (27°) and microcline (28°) peaks. Phyllosilicates (phlogopite and biotite) less intense peaks are observed at 8° (see

Fig. 3.10).



Compound Name	Formula	Y-Scale	I/Ic DB	I/Ic User	S-Q
Quartz low	O2 Si	92.6459 %	4.820		53.90 %
Microcline	Al1.03 K0.986 Na0.014 O8 Si2.97	7.4813 %	0.730		28.74 %
Phlogopite	Fe H2 K0.9 Mg3 Mn0.1 O12 Si3	1.7820 %	0.630		7.93 %
Biotite	Al1.322 Fe0.864 KMg1.638 O12 Si2.84 Ti0.336	5.0399 %	1.500		9.42 %

Mineral phase	Weight %
Quartz	53.9
Microcline	28.7
Phlogopite	7.9
Biotite	9.4

**Fig. 3.10** An example of XRD results analysis based on sample W-1

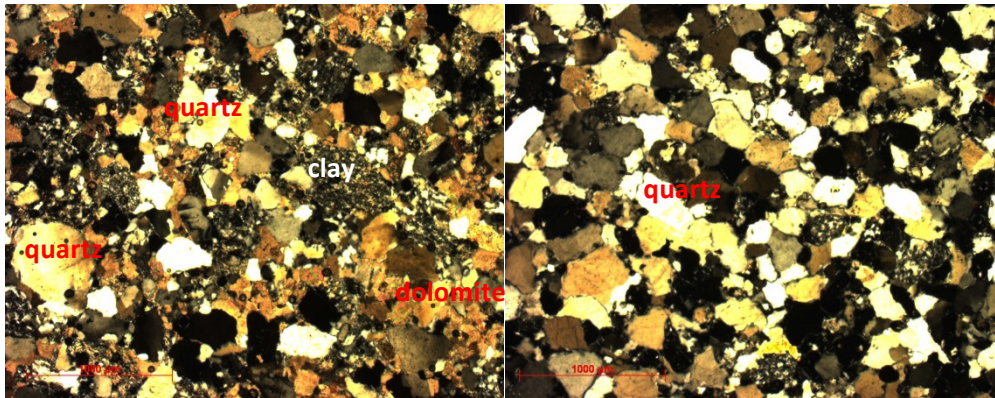
### Q16-02

*Optical microscope images.* The thin sections for Q16-02 representations were obtained from 4 different interval of the bore core, specifically from the top and bottom of each interval.

Q16-02 presents a similar mineral assemblage to W1 bearing quartz, microcline, clay deriving from alteration and accessories which have not been further analysed. However, this sample contain dolomite Ca,Mg (CO<sub>3</sub>)<sub>2</sub> (see XRD) and calcite (CaCO<sub>3</sub>) which occurs in form of grains and cement between the minerals forming the rocks. Carbonate

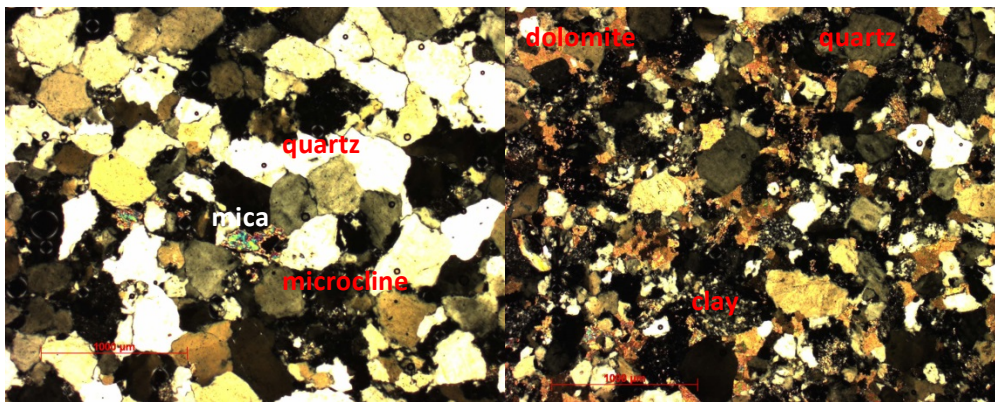
kennisagenda Aardwarmte: Soft stimulation techniques - D2

phases can be observed in Fig. 3.11a and Fig. 3.11d. Fig. 3.11b and c show the typical sandstone texture with the abundance of quartz and microcline grain.



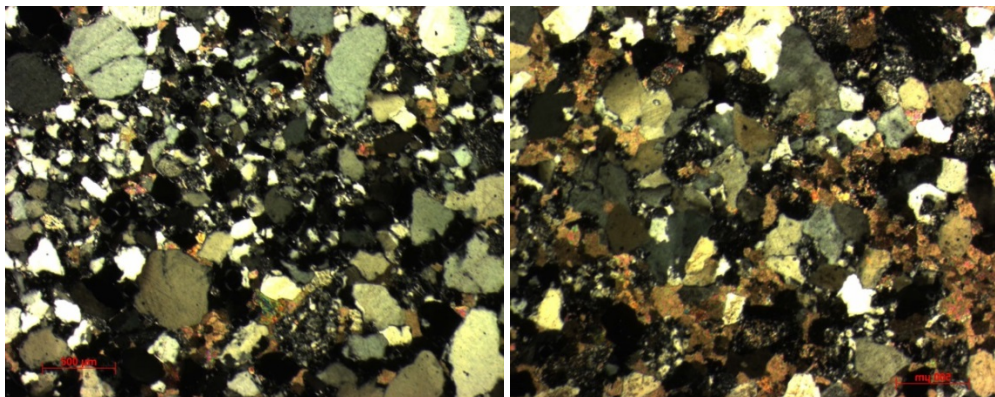
(a) Sample Q16-02 Interval 2 (down)

(b) Sample Q16-02 Interval 1 (down)



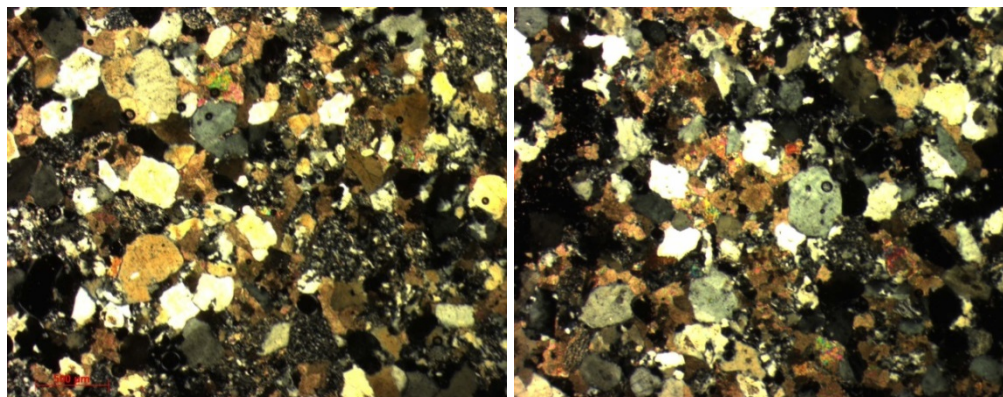
(c) Sample Q16-02 Interval 1(up)

(d) Sample Q16-02 Interval 2(up)



(e) Sample Q16-02 Interval 1(up)

(f) Sample Q16-02 Interval 3 (down)

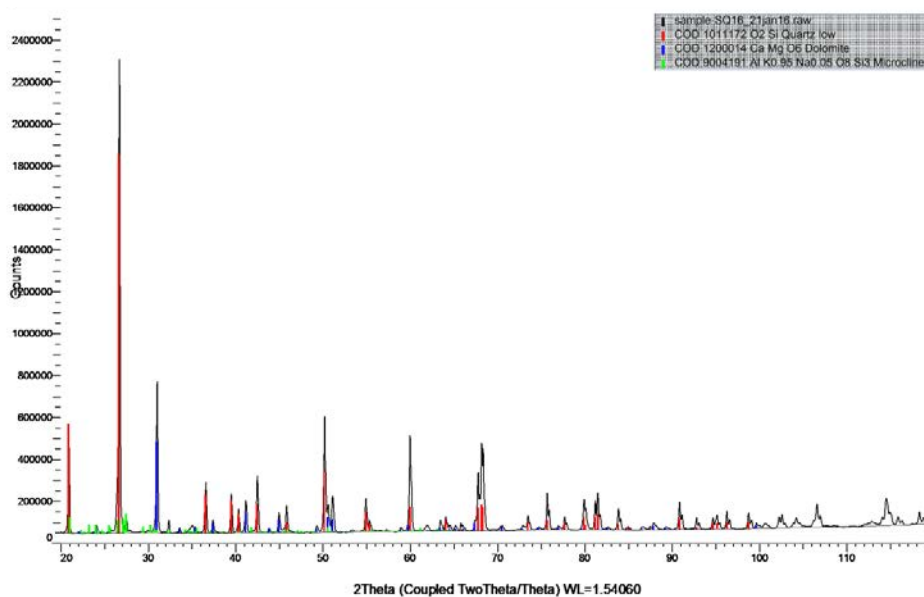


(g) Sample Q16-02 Interval 4(up)

(h) Sample Q16-02 Interval 4(up)

**Fig. 3.11** Optical representation of sample Q16-02 (Intervals 1-4)

**XRD.** The XRD pattern of Q16-02 shows the main quartz peak ( $2\theta=28^\circ$ ) which may be observed in red. As second mineral phase dolomite, previously described in the microscope section, appears with its major peak at  $2\theta=31^\circ$ . Quartz is the most abundant mineral in the sample followed by microcline as listed in the table below.



Compound Name	Formula	Y-Scale	I/Ic DB	I/Ic User	S-Q	Added Reference	d x by
Quartz low	O2 Si	80.0675 %	4.640		55.69 %		1.0000
Dolomite	Ca Mg O6	19.2481 %	2.690		23.09 %		1.0000
Microcline	Al K0.95 Na0.05 O8 Si3	4.1404 %	0.630		21.21 %		1.0000

Mineral phase	Weight %
Quartz	55.7
Dolomite	23.1
Microcline	21.2

**Fig. 3.12** An example of XRD results analysis based on sample Q16-02

### 3.1.2 Fluids

#### 3.1.2.1 Fluid selection

Application of a proper acid is a challenging issue in the soft stimulation technics. Firstly, due to the fact that sandstones are complex rocks of heterogeneous character. Secondly, the temperature variation and the surface morphology of the grains strongly influence the interaction and the effectiveness of the injected fluid. The commonly used solvents are hydrochloric acid (HCl) and as well mixtures of HF/HCl depending on the formation mineralogy and porosity/permeability properties.

In the sandstone formations, where carbonates are present, the HCl is used as an effective agent for creating a new flow path. Nevertheless, most of the sandstone formations are sensitive to HCl, what can result in the formation damage. It has to be noted that all clays have a temperature above which they become unstable in the presence of HCl. When the clay structure is contacted by HCl, it may become disintegrated and release of metal ions can occur resulting in secondary and tertiary reaction products.

The reservoir where the acid injections are planned is located in the temperature regime above 120 °C and contains minerals (see section 3.1.1.3) that in the results of contact with HCl at so high temperatures may cause formation damage (Fig. 3.13). For example, chlorite shows instability already at temperatures above 52 °C. Moreover, all HCl may be spent for disintegrated clays.

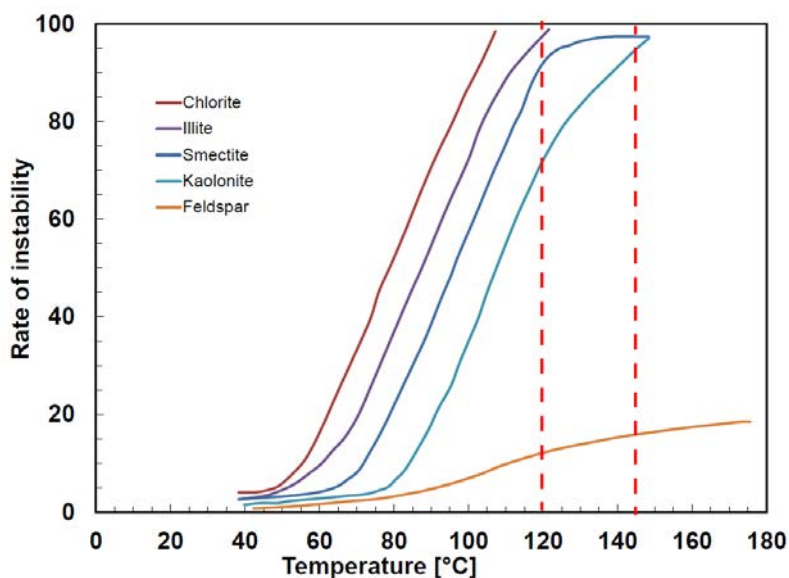


**Fig. 3.13** Sensitivity of various minerals being in contact with HCl over the range of the temperatures. Red box indicate the conditions of the reservoirs discussed in this study.

Another issue is the highly corrosive nature of HCl. If corrosion might occur additives should be used to minimize the effect. However at high temperatures, the efficiency of corrosion inhibitors is reduced together with increasing acid/rock reaction rate which requires the use of a retarded acid system to ensure that the acid is not spent immediately close to the wellbore, but will penetrate deeper into the formation. At higher temperatures, fast reaction occurs between HCl and the calcite minerals leading to rock dissolution and face dissolution.

Due to the complex composition of the samples and possible precipices, if in contact with HCl, we decided to look for another possible solvent. For high temperature reservoirs, chelating agents or aminocarboxylic acids are used as an alternative solution. In research, solvents like GLDA and HEDTA, exhibit several advantages compared to standard systems. For example, they achieve lower reaction rate and by that obtain deeper penetration into the

formation, they are very low corrosively, exhibit satisfactory iron control, thermal stability, and are environmentally friendly. The disadvantage is that they are more costly than standard solutions.

### 3.1.2.2 Operational fluids

In the conducted experiments, the operational saturating phase was brine, and the acid stimulating phase was chelating agent. *Brine*. Synthetic brine used in this study was represented by degassed, demineralized water with 1 M potassium chloride (KCl). The composition of the brine was chosen in order to avoid any problems of clay destabilization and mimic the reservoir history and conditions. Chelating agent H2GLDA is in the form of a diluted solution (50%vol). The viscosity of the chelating agent at experimental conditions is presented in Fig. 3.14.

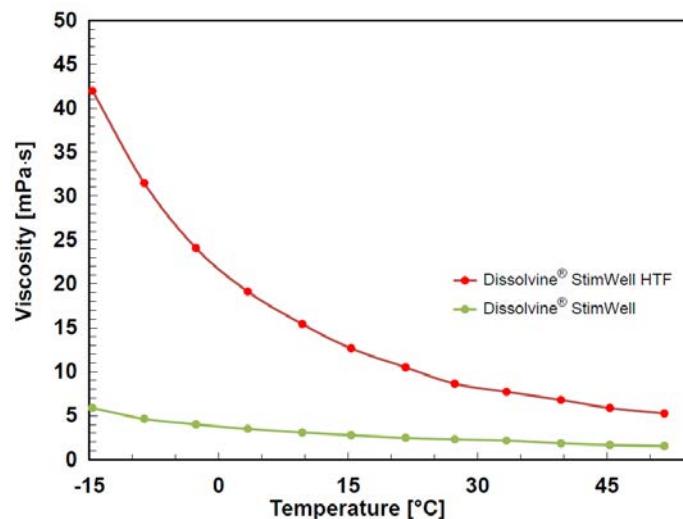
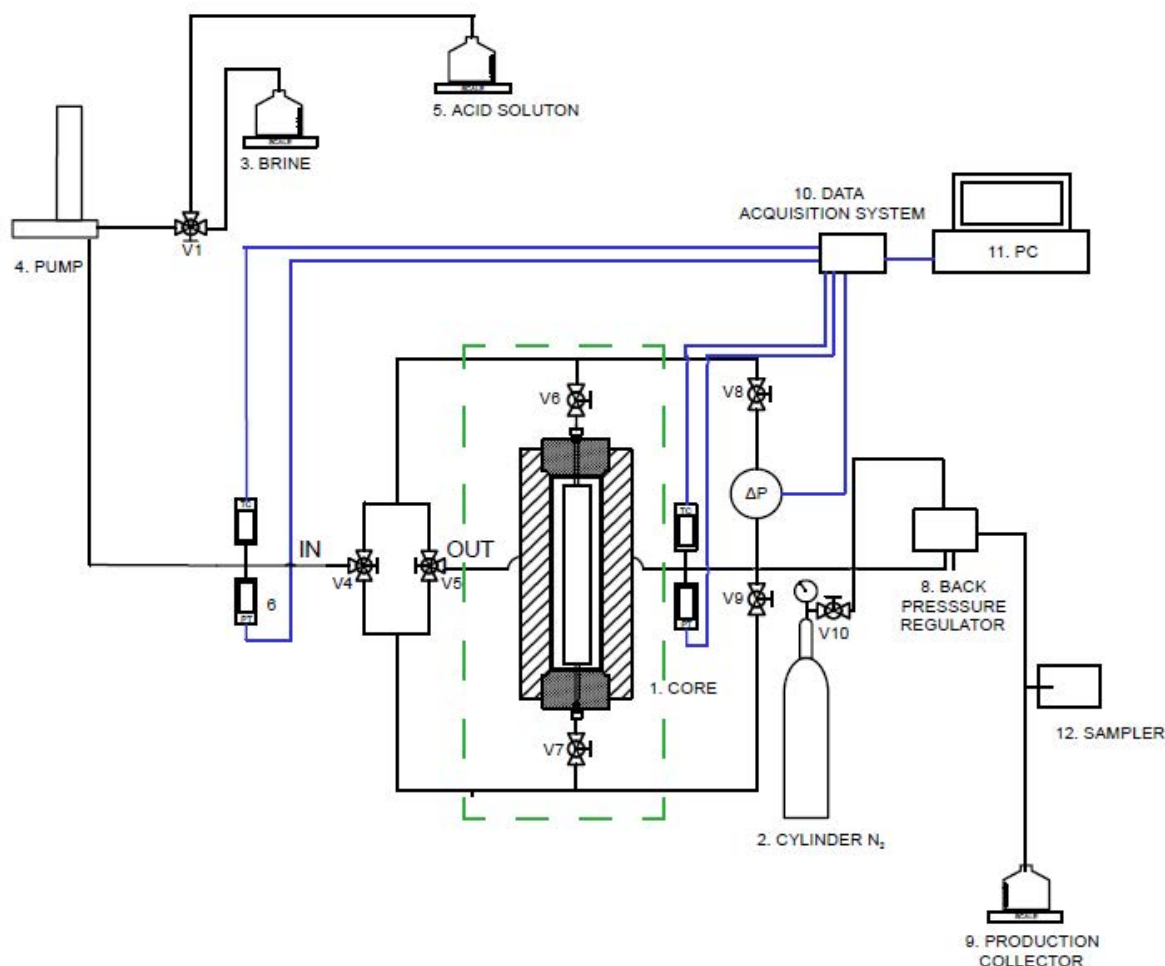


Fig. 3.14 The viscosity of H2GLDA and 50 % vol diluted H2GLDA as a function of temperature.

### 3.1.3 Experimental approach for acid injection into intact rock

#### 3.1.3.1 Experimental set up

The experimental set up was designed and built to conduct quantitative and accurate measurements of produced fluids and gases and to monitor differential pressures across the core (Fig. 3.15). Used cores have dimensions of 3.8 cm in diameter and 9 cm in length. A high pressure PEEK core holder was used to maintain the centralized vertical position of the core. Axial and radial confining pressure was applied through the core holder wall, along the outer diameter of the core samples. Moreover, the flow distribution plugs that remain in contact with a sample were used together with the end caps at the bottom and at top of the core holder. The ISCO pump was used to pressurize the system, inject brine and subsequently inject chelating agent. The ISCO pump was further connected to the bottom side of the core holder. The pressure in the system was maintained by the nitrogen back pressure regulator embedded in the production of the system. The pressure and pressure difference was measured by a system of pressure gates before and after the core. The production line lead to a fracture collector or/and graduated glass tube, where the produced fluids and gas were collected and separated at room conditions. The effluents are collected at the outlet at regular intervals and are further analyzed by the use of Inductively Coupled Plasma atomic/optical emission Spectrometry. The required temperatures were achieved by using an oven in which the core holder was placed with a string shaped inlet core connection to maintain the temperature. To control the pressure and temperature, a pressure transducer and a thermocouple were placed at the inlet and close to the back pressure. The flooding process was constantly monitored and recorded.



**Fig. 3.15** Schematic description of the experimental setup to study matrix acidizing in the sandstones. The green line represents the oven in which part of the experimental setup was built. The black lines illustrate the tubing and the various flow lines. The blue lines are data cables connecting pressure transducers and thermocouples to a computer for acquisition and controlling.

### 3.1.3.2 Experimental procedure

*Initial core saturation.* The sandstone core-plug was initially vacuumed to remove the air and  $\text{CO}_2$ . Subsequently, the 0.1 M KCl brine was introduced to mimic the fluids in the field. First, brine was injected with a constant flow rate of 0.005 ml/min ( $8.33 \times 10^{-11} \text{ m}^3/\text{s}$ ) to the bottom of the core at the ambient injection conditions (room temperature and atmospheric pressure). Then, the tests system was slowly pressurized to 20 bar. 10 PV of brine were injected through the core to achieve complete dissolution and removal of remaining  $\text{CO}_2$  and the full brine saturation of the core-plug. Brine production was connected to the production container and monitored by a scale. Permeability was determined by measuring pressure drops.

*Chelating agent injection.* After brine injection, flooding was switched to the chelating agent with constant flow rate of 0.005 ml/min ( $8.33 \times 10^{-11} \text{ m}^3/\text{s}$ ). The outlet was connected to the production collector placed on the scale. It allowed to monitor exact volume of injected and produced fluid. Moreover at the constant intervals, fluid samples were collected at the outlet in purpose of density measurements.

*Brine post flood.* The fractured sandstone core-plug was brine flooded with 20 PV (pore volumes) of de-aired brine at 0.005 ml/min in order to obtain the same conditions as at the beginning of the experiment.

### 3.1.4 Experimental approach for acid injection into fractured rock with a control over the confining pressure

#### 3.1.4.1 Experimental set up

The setup consisted of two parts: (1) fracture developer and (2) the flooding system.

The artificial fractures were created using a special instrument for the stress application to the samples of different dimensions (Fig. 3.16). In this study, cylindrical samples were placed in the instrument and single fractures were created along the main axes of the sample.

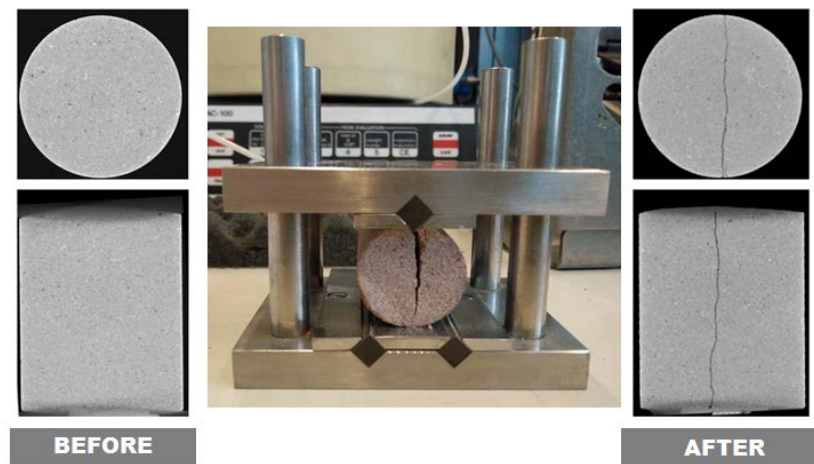


**Fig. 3.16** Instrument for artificial, single fracture creation (middle) and an example of a sample in which fracture was developed (left and right).

*Acid injection into fractured rock.* The experimental setup for acid injection was built in similar manner as the setup for the injection into the intact rock (Fig. 3.17). The main difference is that the axial and radial confining pressure chamber of the PEEK core holder is separated from the flow system (Fig. 3.18). The pressure within the chamber is controlled by a supply of nitrogen. Moreover, a confining pressure sleeve (material: rubber/teflon depending on the temperature conditions) surrounds the outer diameter of the fractured core sample. Pressure drop is measured along the length of the core sample through a pressure difference apparatus. The ISCO pump was used to pressurize the system, inject brine and subsequently inject chelating agent to the system. The ISCO pump was further connected to the bottom side of the core holder. *Injection system.* The fluid in the pump was preheated to the experimental conditions and the connection to the system was isolated in order to avoid changes of the phase's behavior. The production system lead by a line to an inline density meter and further to a fracture collector, where the fluid was collected and gas was separated at the room conditions. The collected samples were analyzed by the use of Inductively Coupled Plasma atomic/optical emission Spectrometry. The required temperatures were achieved by using a double 'growth tent' that behave in a similar way as an oven and can be placed on a table of the medical CT-scanner.

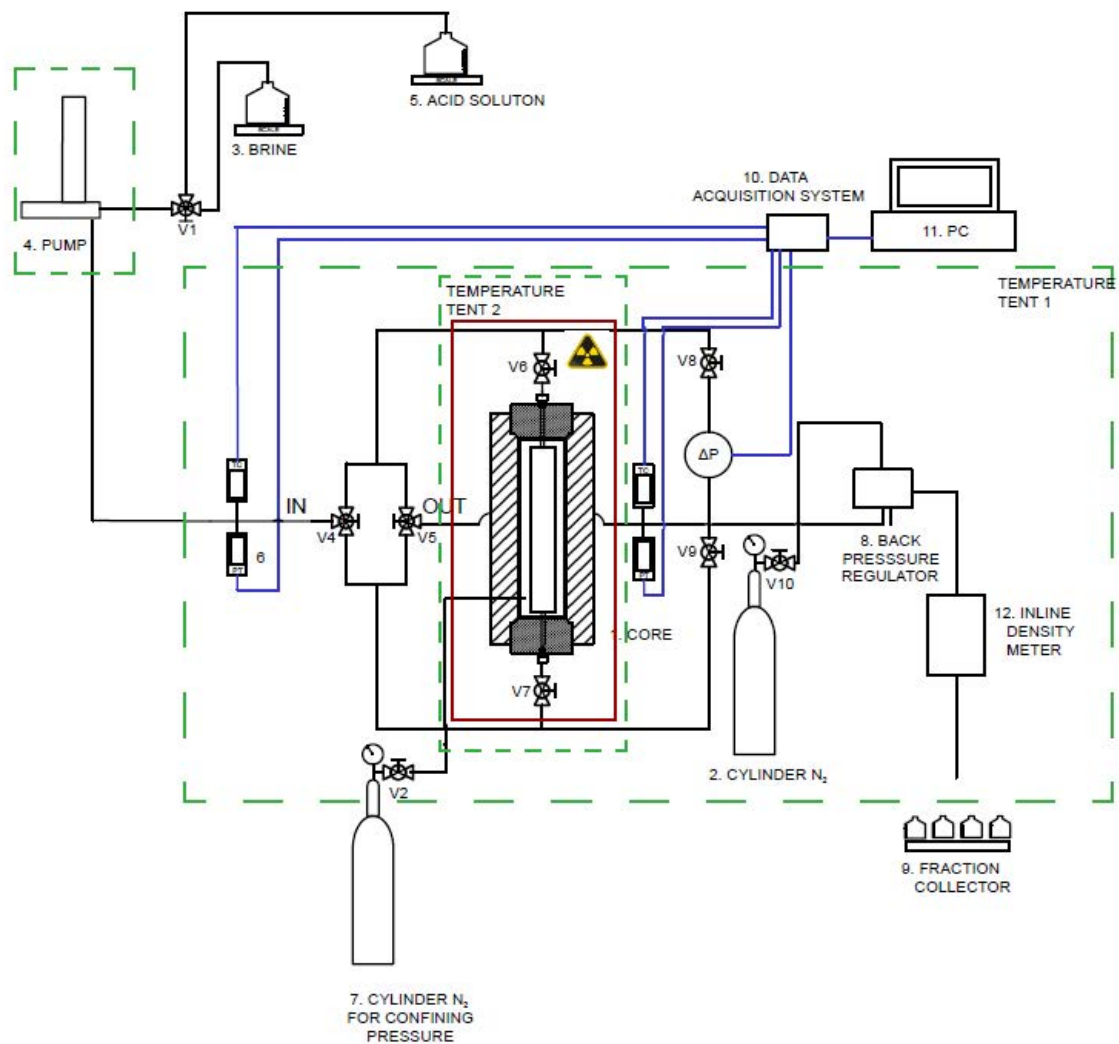


**Fig. 3.17** Schematic description of the experimental setup to study matrix acidizing in the fracture sandstones. The green lines represent the thermal box in which the experimental setup was built. The black lines illustrate the tubing and the various flow lines. The blue lines are data cables connecting pressure transducers and thermocouples to a computer for acquisition and controlling.

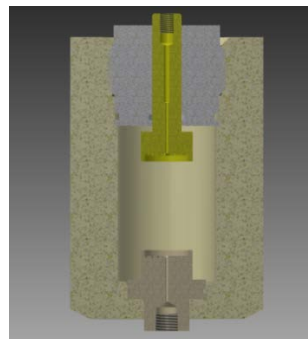


**Fig. 3.18** Schematic representation of the PEEK core holder with the external system for the confining pressure control.

### 3.1.4.2 Experimental procedure

*Initial core saturation.* The sandstone core-plug was initially vacuumed to remove gas from the pore space (air and CO<sub>2</sub>) and after the brine flooding was introduced (0.1 ml/min). First, brine was injected to the core at the ambient injection condition (back pressure at atmospheric pressure) and confining pressure of 30 bar. Subsequently, the pore system was slowly pressurized to 15 bar back pressure. 10 PV of brine were injected through the core to achieve: (1) a complete dissolution and removal of remaining CO<sub>2</sub> and (2) a full brine saturation of the core-plug. Brine production was connected to the production container and monitored by a scale. Permeability was determined by measuring pressure drops over the core.

*Chelating agent injection.* After the brine injection, flooding was switched to the chelating agent with flow rate 0.1 ml/min. The outlet was connected to the fraction collector and density meter that allowed monitoring of the exact volume of produced CO<sub>2</sub>.

*Confining pressure variation.* Confining pressure around the samples was varied (first increased and further decreased) in order to investigate the hydro-mechanical behavior. Fracture aperture controls the amount of fluid flowing through a fracture. By varying confining pressure, a relation between a fracture aperture increase due to dissolution and fracture aperture decrease due to incremental stress was investigated.

*Brine post flood.* In order to obtain the same experimental conditions as at the beginning of the experiment (at confining pressure of 30 bar) the fractured sandstone core-plug was brine flooded with 60 PV (pore volumes) of de-aired brine at 0.1 ml/min.

*Dual energy CT scanning.* The behavior of the fractured rock under the different confining conditions was monitored by using X-ray scanning technique with a third generation SAMATOM Volume Zoom Quad slice scanner. The scans were performed at two different energy levels. Table 3 shows the imaging settings used in the experiments.

**Table 3** The overview of the settings of CT scan measurements.

Specification	Quantity
Tube voltage (kV)	20, 140
Tube current (mA)	250
Scan mode	Sequence
Image extent (voxels)	512 x 512 x 36

## 4 Numerical model results

### 4.1 Core scale model

The available reactive surface area value is changed within the limits from literature to obtain a match between the experimental and numerical results. The same determined value of the available reactive surface area is maintained throughout the rest of the modelling process. For the consistency of the results, all the plots in this section were obtained for injection of 13.6 wt% HCl.

#### 4.1.1 Effect of calcite concentration

The plot in Fig. 4.1 shows the effect of increasing calcite concentration on the permeability – porosity plot in core scale. As the calcite fraction increases the dissolution increases and so does the permeability and porosity accordingly. It is also important to notice the two different slopes in Fig. 4.2. The initial slope represents the period when the acid front has not reached the outlet, representing phase dissolution. The second slope represents the period where the acid front has reached the outlet and uniform dissolution takes place resulting in a great increase in permeability. Fig. 4.2 shows the effect of calcite concentration on the scaled permeability relationship.

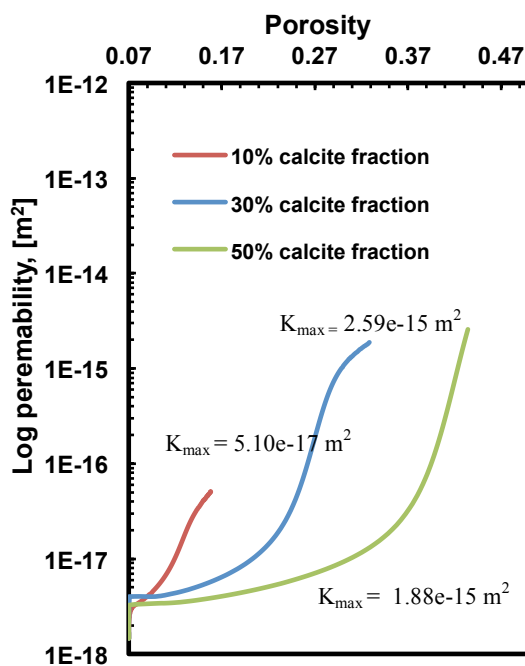


Fig. 4.1 Effect of calcite concentration on the permeability - porosity plot.

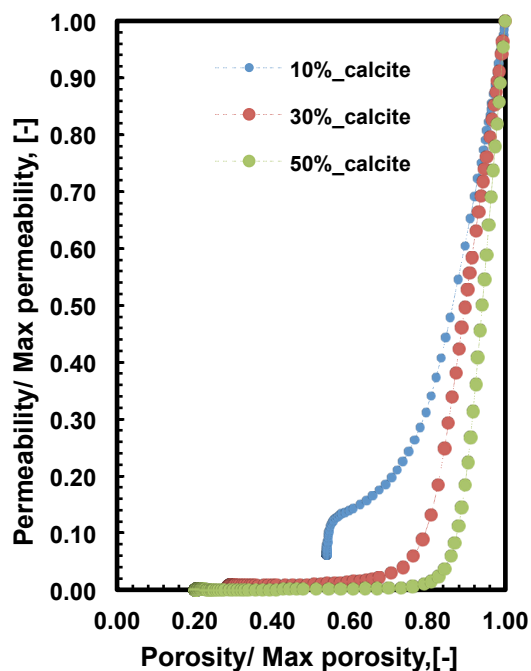


Fig. 4.2 Effect of calcite concentration on a scaled permeability against scaled porosity plot.

#### 4.1.2 Effect of temperature

The effect of temperature on calcite dissolution for a core scale model is given in Fig 4.3. The plot shows the permeability-porosity development for injection of HCl for an initial calcite concentration of 10%. With increasing temperature, the rate of reaction increases, thus improving the permeability development across the core for the same volume of acid injected. Although a temperature related trend is observed, the final permeability would be the same in a homogeneous case, as the calcite present is assumed to be accessible to the acid.

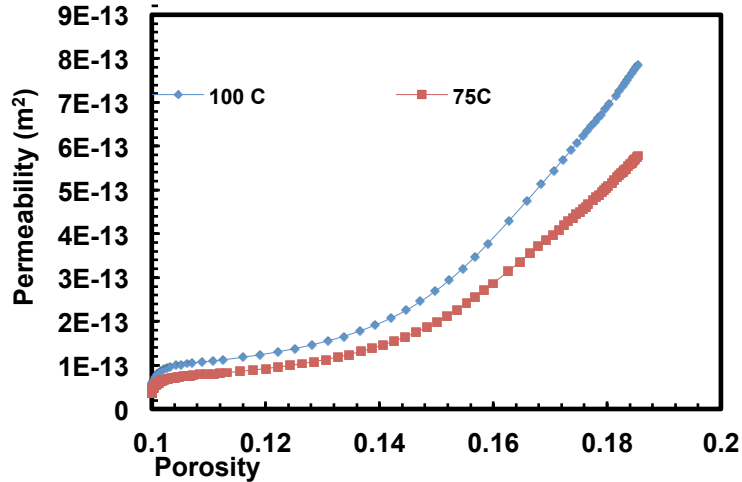


Fig. 4.3 Effect of temperature on core scale model for 10% calcite fraction.

#### 4.1.3 Effect of injection rate

The effect of varying injection rates for the same volume of acid injected is analyzed on the core scale model. The injection rate is an important parameter that determines the type of a dissolution. The existence of an optimum injection rate, a well-established phenomenon in carbonate reservoirs, has been established (Fred et al., 1999). At extremely low flow rates, most of the dissolution takes place close to the injection point and it might not have an effect on the overall permeability. This dependency of dissolution pattern on flow rate is very common in carbonates as in carbonates the whole matrix is being dissolved. In the case of sandstones, it might be important depending on the amount of calcite available and many other parameters. An example for the dependence of carbonate dissolution patterns on the injection rate is given in Fig. 4.4.

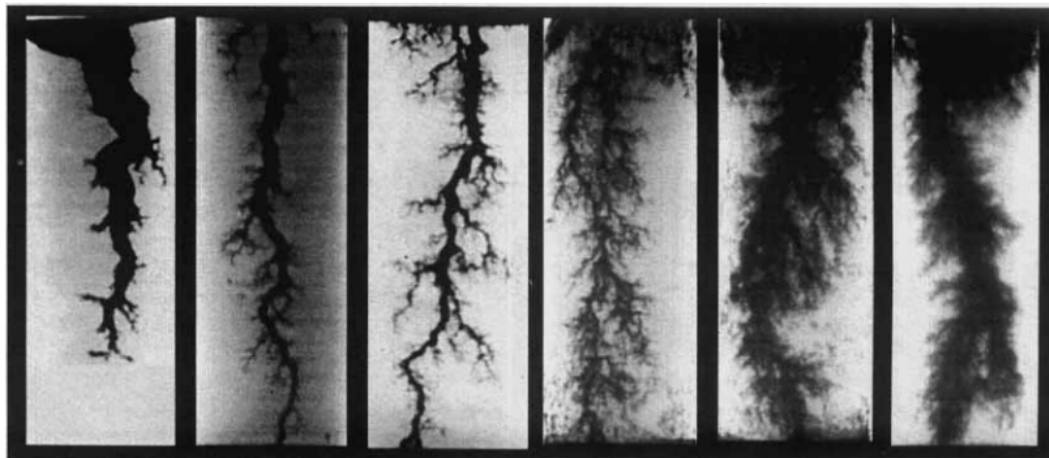


Fig. 4.4 Dependence of the dissolution patterns on injection rates.

The effect of different injection rates on a sandstone core scale permeability-porosity relationship is analyzed. Although the effect of the flow rate is a very important parameter in carbonate reservoirs, there is no significant change observed for varying flow rates in our case. It is also important to understand that modelling the creation of wormholes is a very complex process that requires detailed modelling.

## 4.2 Homogeneous system

In this section, the average value of the available reactive surface area obtained from the core scale model has been used to analyze the effect of calcite dissolution in a homogeneous field. This part of the model is done under the assumption of a homogeneous field with constant permeability and porosity value throughout. The heat loss during geothermal production is not considered in this section and will be discussed later in the heterogeneous model. All the plots shown in this section were obtained for 13.6 wt% HCl injection.

### 4.2.1 Effect of calcite concentration

The effect of calcite concentration on the radius of influence is shown in Fig. 4.5. The radius of influence is defined as the radius surrounding the wellbore that has permeability improvement. In this case for a constant volume of acid injected, the radius of influence is defined as the radius at which the permeability falls below 30% of the maximum permeability achieved.

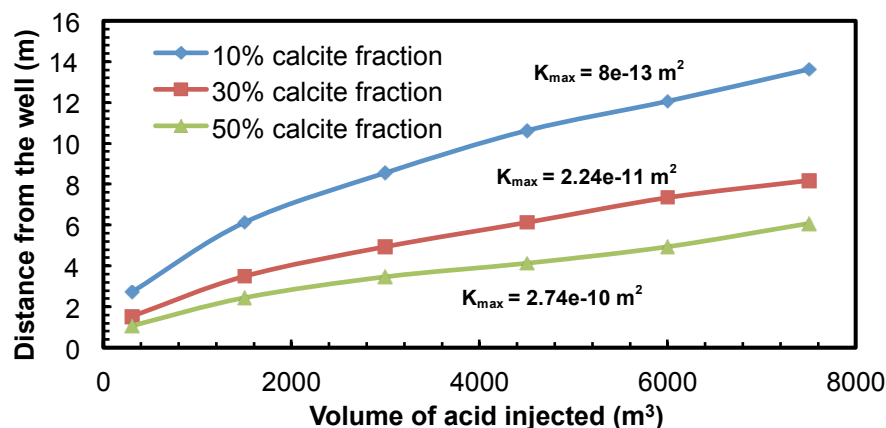


Fig. 4.5 Effect of calcite concentration on the radius of influence as a function of the volume of acid injected.

Table 4 Effect of calcite concentration for a constant volume of acid injected as a function of the radius of influence.

Volume of acid injected(m <sup>3</sup> )	300	1500	3000	4500	6000	7500
% calcite	Distance from the well (m)					
10	2.72	6.13	8.56	10.63	12.07	13.63
30	1.54	3.49	4.94	6.13	7.35	8.19
50	1.07	2.45	3.47	4.14	4.95	5.77

From the Fig. 4.5 and

Table 4, for a constant volume of acid injected it can be observed that as the calcite concentration increases the reactions taking place close to the well increases and therefore increasing the amount of acid spent close to the wellbore. This, in turn, implies that with the dissolution of calcite increasing close to the wellbore, the porosity and permeability increase close to the wellbore. This effect can be observed clearly in Fig. 4.6 and Fig. 4.7, which shows the effect of changing calcite concentration as a function of log-scale permeability close to the wellbore.

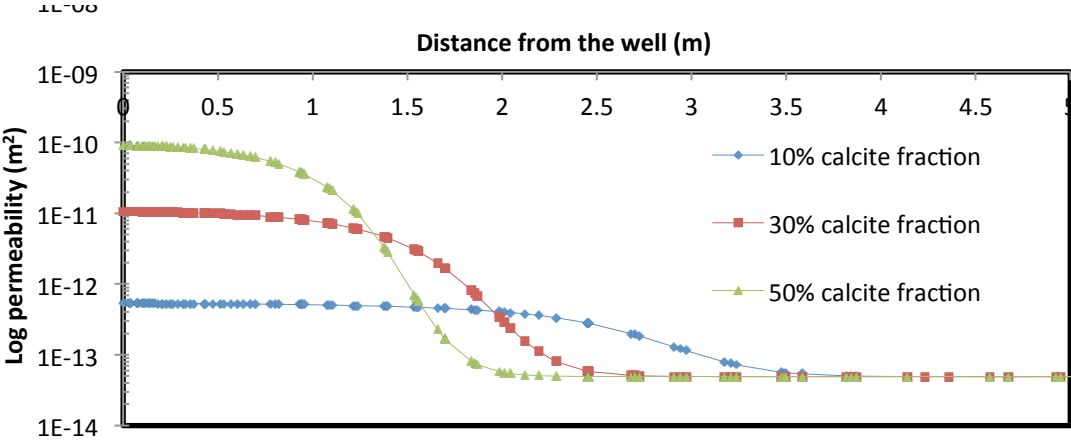


Fig. 4.6 Effect of calcite concentration on the permeability as a function of the distance from the well after 10 hours of acid injection.

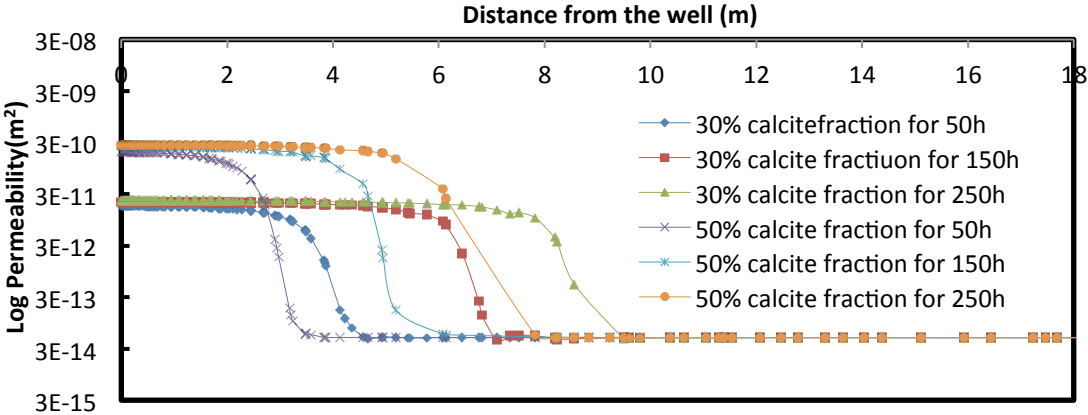


Fig. 4.7 Effect of calcite concentration on the permeability as a function of the distance from the well at different volume of HCl injected.

According to Fig. 4.7, the penetration depth of acid (acid front) and the permeability of the region surrounding the wellbore increase as the volume of injected acid is increased. However, the increase in permeability is not linearly correlated to the volume of acid injected. For example, by increasing the acid volume from 1500 m³ to 7500 m³, the penetration depth increases from 4 m to 9 m away from the wellbore. This is attributed to the fact that at the field scale, the flow is essentially radial, whereas core flood data are obtained for the linear flow of acid in a confined porous medium. Note that this conclusion is valid for the conditions considered, i.e. the uniform distribution of dissolvable material and uniform dissolution at the acid front.

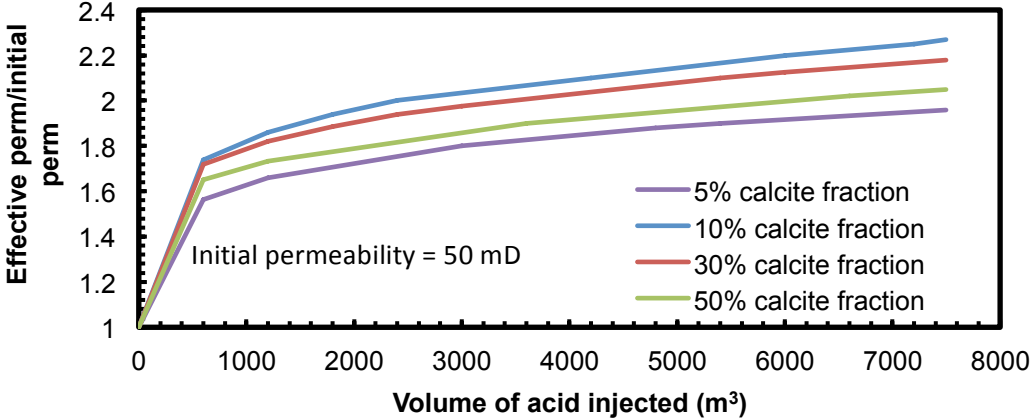


Fig. 4.8 Effect of calcite concentration on scaled permeability as a function of volume of acid injected.

Fig. 4.8 shows the equivalent permeability for a certain volume of volume injected assuming a constant porosity value of 10%. Equivalent permeability obtained for a certain volume of acid injected can be calculated by increasing the initial permeability in a homogeneous system such that the pressure difference between the two wells is equal to the pressure difference obtained after stimulation. This could be used as an indicator of the effect of acid stimulation between the two wells.

It can be observed (Fig. 4.8) that the equivalent permeability for a lower calcite fraction is higher when compared to that of a greater calcite fraction except for the 5% calcite concentration case. As explained earlier, in a homogeneous system, the amount of calcite dissolved close to the wellbore increases with increasing calcite concentration and hence consuming greater amounts of acid. This implies that the radius of influence for a homogeneous system with 10% calcite concentration is greater than that obtained for a system with 30% calcite concentration. Although in the case of 5% calcite concentration the acid penetration is the highest, the amount of permeability increase is too low to have the expected impact on the Equivalent permeability.

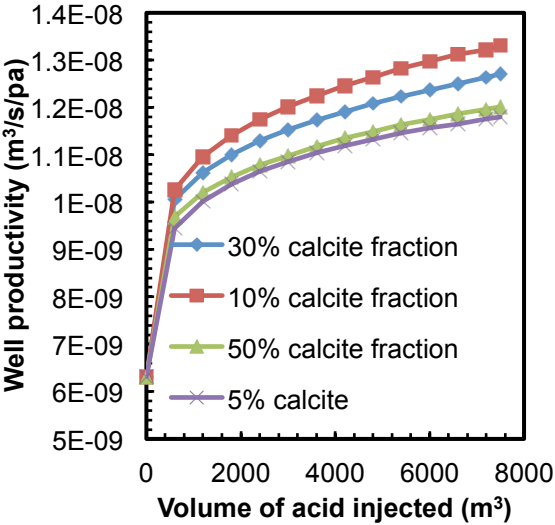


Fig. 4.9 Effect of calcite concentration on the well productivity as a function of the volume of acid injected.

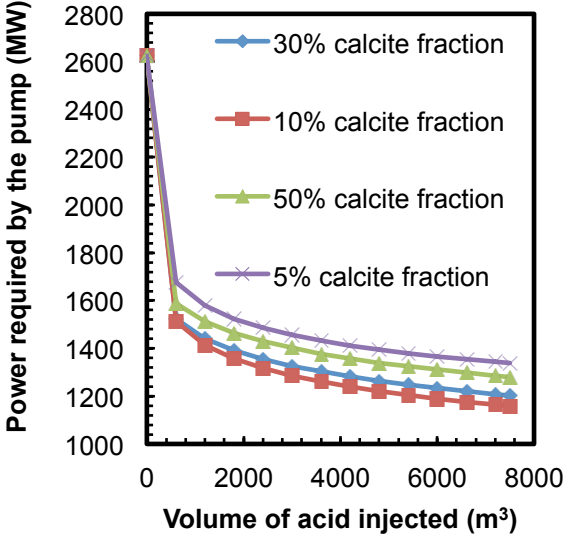


Fig. 4.10 Effect of calcite concentration on power required by the pump as a function of the volume of the acid injected

**Fig. 4.9** Effect of calcite concentration on the well productivity as a function of the volume of acid injected.

**Fig. 4.10** Effect of calcite concentration on power required by the pump as a function of the volume of the acid injected

Fig. 4.9 shows the well productivity or productivity index versus the injected volume of stimulating fluid. The productivity index (PI) expresses the ability of a reservoir to deliver the fluid to the wellbore. The productivity index of a well can be given by

$$PI = \frac{Flow\ rate}{(Average\ reservoir\ pressure - Well\ pressure)}$$

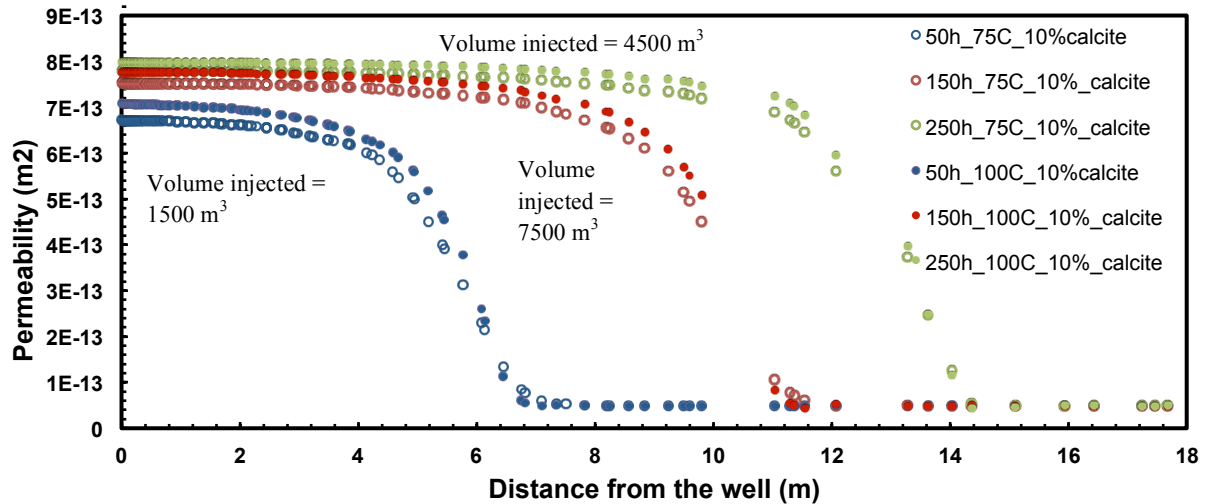


**Fig. 4.11** Effect of temperature on the permeability as a function of the distance from the well for different temperatures.

As the productivity index increases, the total liquid flowrate to the surface increases for a given pressure drawdown. This could also be related to the economy of the process as it directly affects the pump power required. Fig. 4.10 shows the effect of the change in calcite concentration on the pump power required for a long term production of a closed loop doublet system as a function of the volume of acid injected respectively. It can be seen from the Figs 4.9 and 4.10 that pump power required and well productivity follow a similar trend as that of the equivalent permeability. Thus, the efficiency of the stimulation process is impacted by both the permeability improvement produced and the penetration of the acid.

#### 4.2.2 Effect of temperature on radius of influence and pump power

For a homogeneous system with constant permeability and porosity, the effect of temperature at which the calcite dissolution takes place is discussed in this section. The system has been analyzed for temperatures of 75 and 100 °C. From the Fig. 4.11, it can be observed that for a constant volume of acid injected the penetration depth and the permeability development increases with temperature. This can be explained by the temperature dependence of the rate of acid-calcite interaction. Thus, the amount of calcite dissolved increases and hence the permeability improvement is better. The increase in penetration depth can be explained by the decreasing viscosity with temperature. As the viscosity is lowered, the ease of flow in the reservoir increases and hence the acid penetration increases.

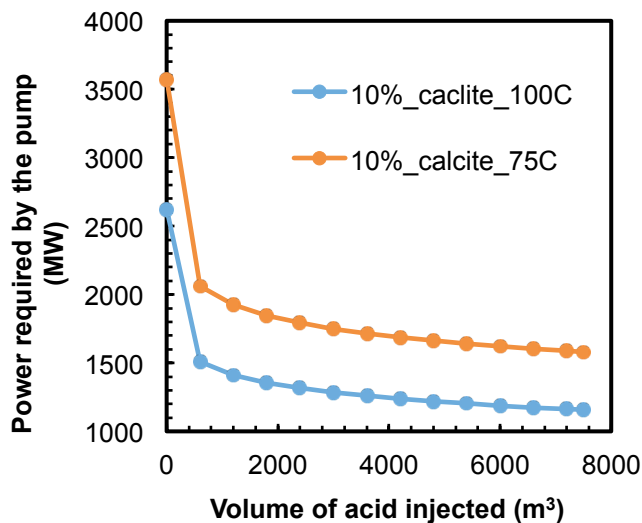


**Fig. 4.12** Effect of temperature on the pump power as a function of the volume of acid injected.

Fig. 4.12 shows the power required by the pump for long term production and the effect of temperature on the well productivity. The well productivity and power required by the pump follows a similar trend as discussed in the earlier case. Temperature has a major effect on the well productivity as well as pump power required. This is due the fact that temperature directly influences the viscosity of the fluid. Thus, the temperature of the field is an important factor affecting the well productivity as it also influences the rate of the acid/rock reaction and thereby influencing the effective reach of the acid injected.

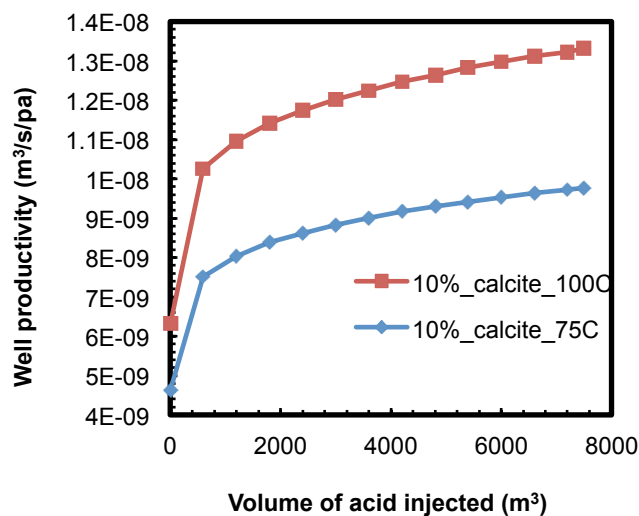


**Fig. 4.13** Effect of temperature on the well productivity as a function of the volume of acid injected.

### 4.3 Heterogeneous model

The effect of calcite dissolution on a heterogeneous field sclaes model is analysed in this section. Further, the water viscosity, thermal conductivity, heat capacity and water density are also defined here as functions of teperature in order to obtain accurate simulations.

#### 4.3.1 Effect of heterogeneity

Heterogeneity was implemented for permeability and porosity similar to Crooijmans et al., (2016). This results in effects like fingering in the acid front which in turn cause an uneven porosity and permeability development. The modeling results show that channelling takes place causing uneven dissolution based on the ability of the acid to flow. This implies that the effective radius of influence is varies based on the heterogeneity in a given direction.

#### 4.3.2 Effect of temperature

The effect of temperature on calcite dissolution over a heterogeneous field is discussed below. The Fig. 4.14 shows the change in well productivity versus the volume of stimulating fluid injected. The Fig. 4.15 shows the effect of different temperatures during calcite dissolution on the pump power required for long term closed loop doublet system production. It can be observed that the well productivity and pump power required follows a similar trend to that of a homogeneous field. Although the pump power required follows a similar trend, the magnitude of the difference seems much less than the homogeneous case.

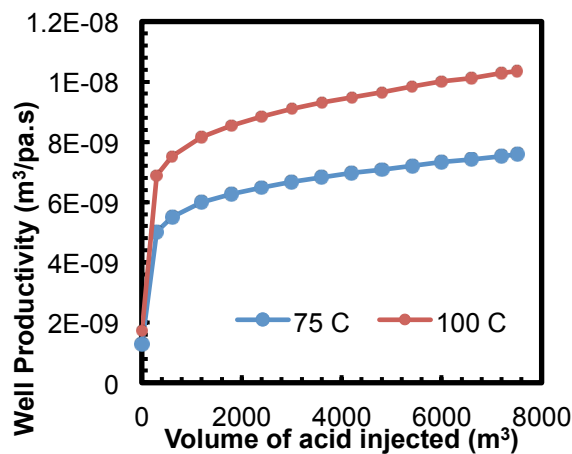


Fig. 4.14 Effect of varying temperature on well productivity and volume of acid injected.

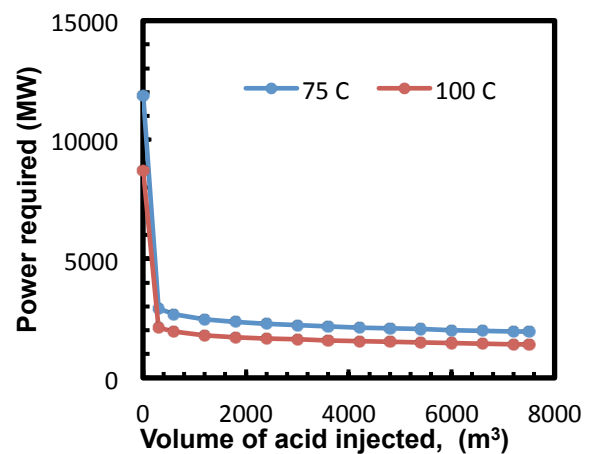


Fig. 4.15 Effect of varying temperature on power required by the pump

#### 4.3.3 Effect of stimulation of field life

Fig. 4.16 shows the effect of acid stimulation on the field life. Acid stimulation may improve the life of a geothermal field by enhancing the permeability in previously impermeable rock.

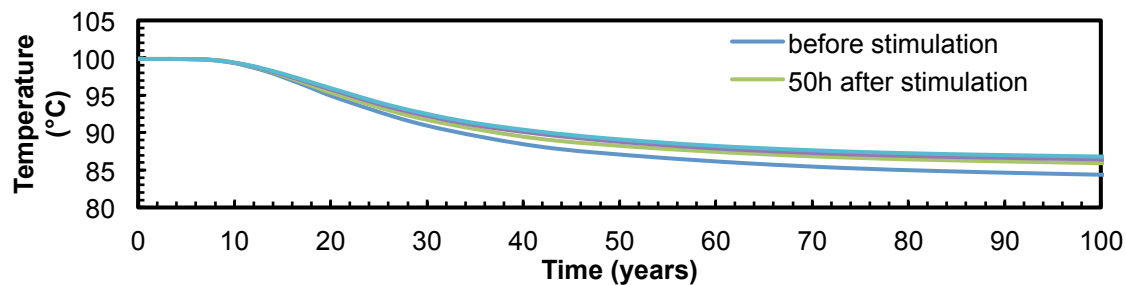


Fig. 4.16 Effect of acid stimulation on field life for different volumes of acid injected.

## 5 Experimental results

### 5.1 Acid injection into intact rock

After the core is saturated with brine, 50 volume % chelating agent is injected with a constant back pressure above 20 bar. Carbon dioxide (CO<sub>2</sub>) gas is released as the calcite in the core is absorbed by the chelating agent. This released CO<sub>2</sub> is dissolved in the liquid phase by the back pressure maintained in the system. The permeability increase in carbonates can be of huge magnitude but in the case of sandstones, it depends on the amount of cementing material available to react with the chelating solution.

Results: Initial permeability = 1.45 μD

Final permeability = 2.10 μD

The porosity changes were too low to be measured with the certainty of being outside the error zone.

### 5.2 Acid injection into fractured rock with a control over the confining pressure

In this section the acid injection into fractured samples is discussed. As shown in section 4.1 the Triassic reservoir is strongly heterogeneous with a non-uniform deposition of carbonates (the main target mineral of the study). Therefore, the main purpose of this sub-study is to compare the behavior of the fractured well samples with varying carbonate content. Note that the fracture geometry differs among the discussed.

#### 5.2.1 Q16-02 well sample - 3630.75 - 3631.33 m

The acid injection tests were conducted on the sample obtained from well Q16-02, interval 3630.75 - 3631.33 m that contain between 12-20wt.% of carbonates. The injection of 50% diluted H2GLD (further in the text called only H2GLD) resulted in a fracture aperture increase and in a permeability increase over 400%. Detailed descriptions of the tests are presented below.

The injection of the H2GLD was introduced after saturating the core with 1M KCl brine and was divided into 3 steps: (1) at back pressure of  $P_{c1} = 30$  bar; (2) at back pressure of  $P_{c2} = 35$  bar; (3) at back pressure  $P_{c3} = 45$  bar. Remaining parameters are kept constant: flow rate of 1ml/min and back pressure of 15 bar. The main purpose of stage 1 was to measure the permeability change in a qualitative and quantitative manner at constant conditions. Steps 2-3 were introduced in order to investigate the behavior of the fracture and further (possible) acidizing process under varying confining conditions.

The three stages of the process over time with application of various confining pressures are illustrated in Fig. 5.1. At stage 1, just after switching the injection from brine to H2GLD, a significant pressure increase in the samples is observed (~4 bar). The main reason is the larger viscosity and density of the chelating agent in comparison to brine (viscosity ~4 times more). However, a chemical reaction occurs as fast as the chelating agent is in contact with rock minerals what may additionally influence the pressure drop respond. At ~0.5 PV injected, a change in the pressure drop is visible, what can be correlated to dissolution of minerals at the fracture surface. After around 27 min (1 PV injected) the pressure drop starts to stabilize at a constant value ( $dp_{lave}=1.2$  bar).

As a result of constant pressure respond, the experiment was moved to stage 2, where confining pressure was increased to 35 bar. Increase of confining pressure in the flow of non-reacting agent results in the closure of the fracture aperture due to a higher confining pressure to injection pressure ratio (see report 1: II.III.II). In this study only a small increase and further decrease in pressure drop respond can be observed at the moment of confining pressure change (Fig. 5.1). Subsequently, pressure rises like at stage 1 (but in a smaller extend) and after injection of 2.5 PV again stable conditions are achieved at a pressure similar to stage 1. It means that the effect of further dissolution and removal of the minerals was stronger than the effect of increased confining pressure. After pressure stabilization the procedure is repeated and the confining pressure is increased.

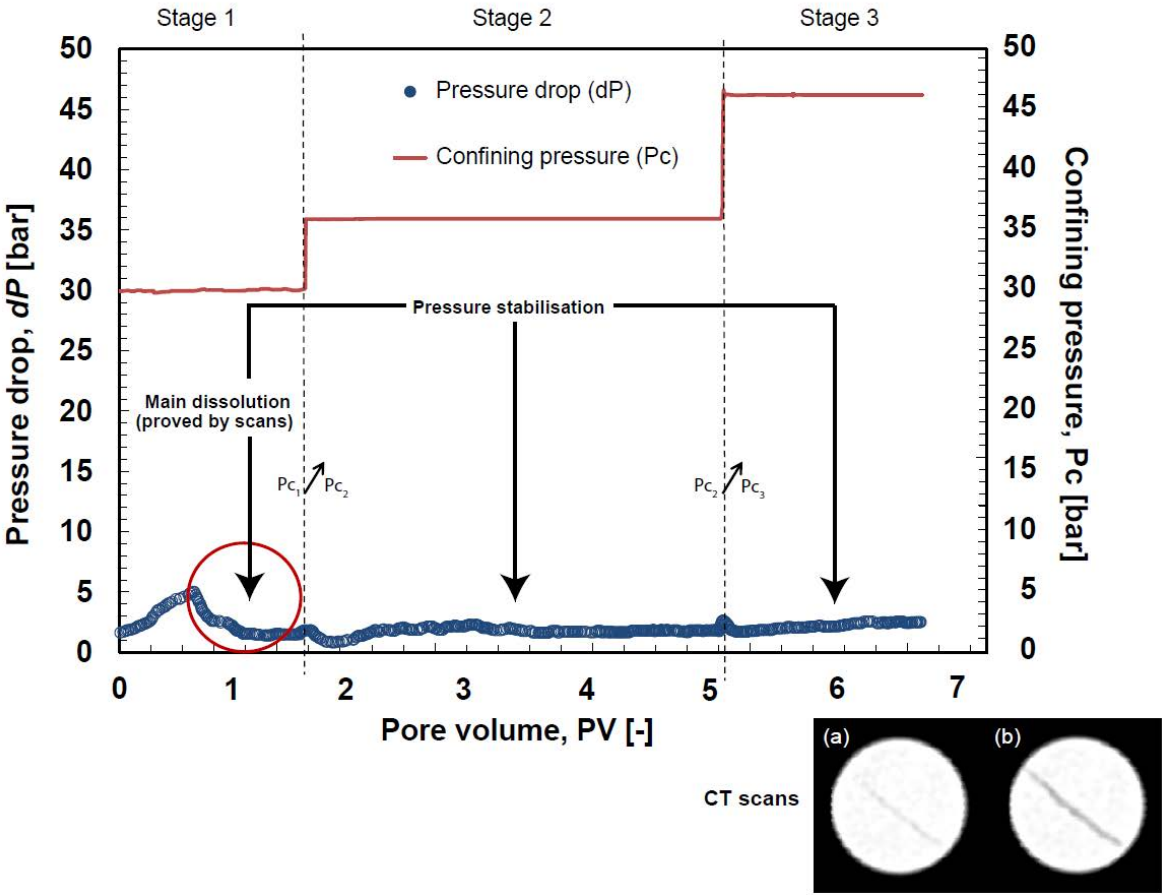
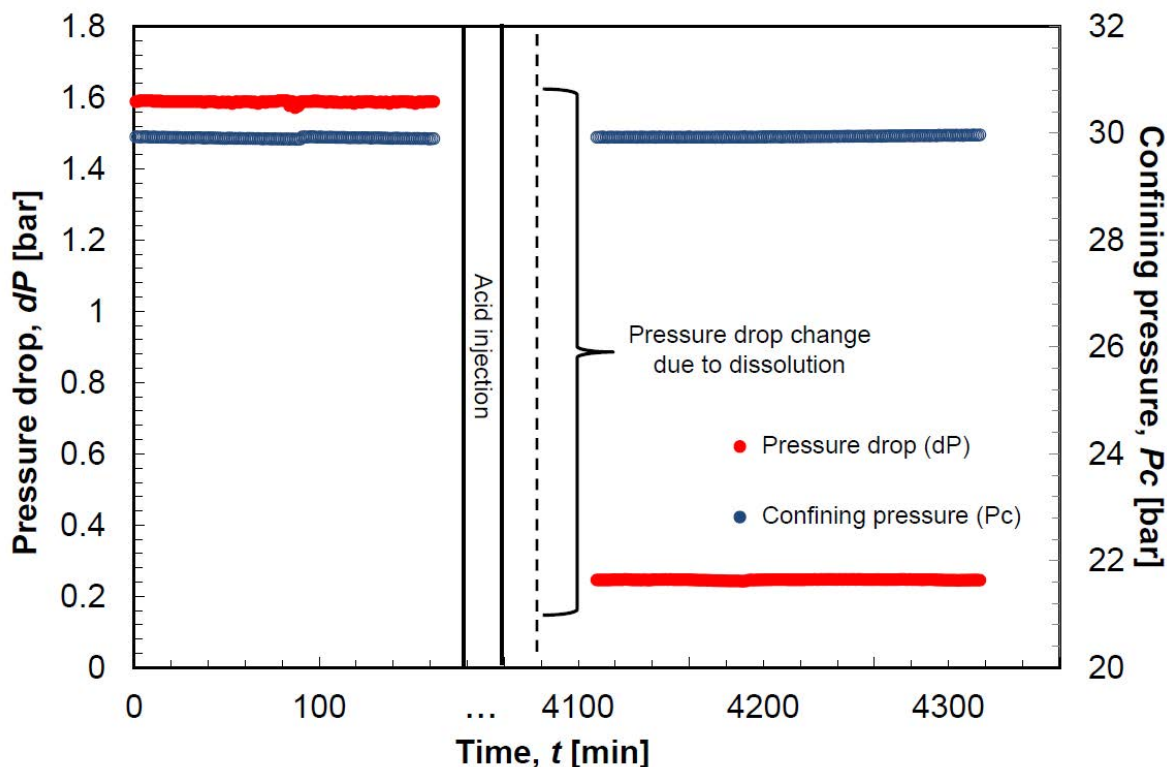
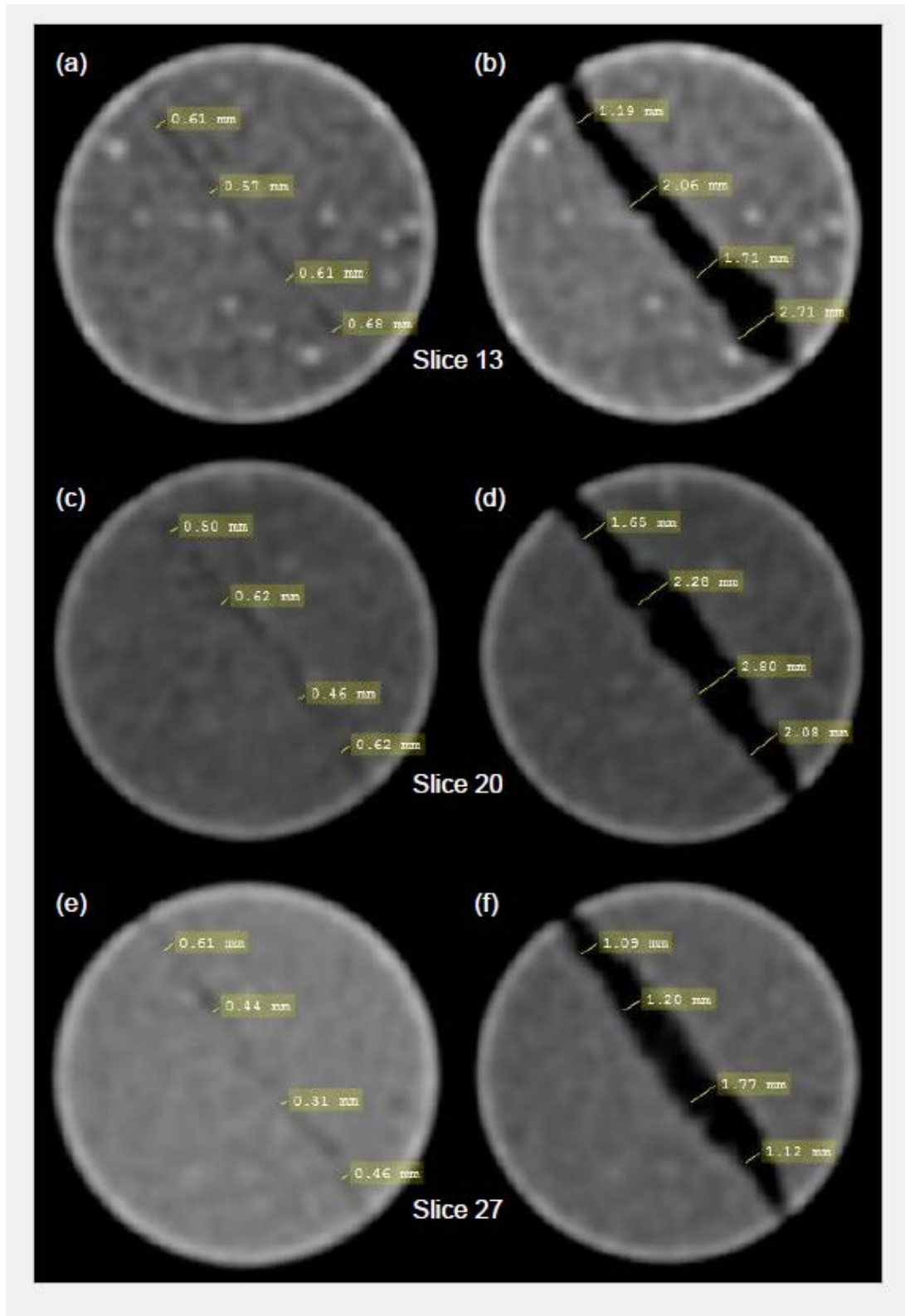


Fig. 5.1 Injection of the H2GLD into the well sample: Q16-02 (3630.75 - 3631.33 m) represented by pressure drop and confining pressure change over injected pore volumes of the fluid.



**Fig. 5.2** Comparison of pressure drop over the core at the same operational conditions (one flowing phase: brine, flow rate 0.1 ml/min, confining pressure 30 bar, back pressure 15 bar) before and after acid injection showing increase in the sample permeability.

The next experimental phase was a brine post flush of the fractured sample at the conditions of stage 3. Further, the system was depressurized to the preliminary conditions of the brine injection. The comparison of the sample respond to brine injection at a flow rate of 0.1 ml/min and a confining pressure of 30 bar (before and after acid injections) is presented in Fig. 5.2 and Fig. 5.3. The measurements and scans called “before” were obtained after preliminary saturation of the sample with brine; scans called “after” were obtained after post-flushing the sample with 60 PV of brine. In order to revise a completion of the displacement of the chelating agent by brine, the density of the effluent fluid was measured. Both Fig. 5.2 and Fig. 5.3 show a significant change in the geometry of the fracture aperture. Fig. 5.2 states a significant decrease in pressure drop (from 1.6 bar to 0.3 bar) and a corresponding permeability increase (from 1.3 mD to 7.1 mD). To visualize the effect, aperture measurements were conducted at 4 locations per cross section, resulting in the comparison included in Fig. Fig. 5.3. It can be observed that the fracture aperture increased significantly (up to 500% depending on the location) as a result of the H2GLD injection and reaction with carbonate minerals.



**Fig. 5.3 (a-f)** CT scans visualisation of the fracture aperture change over 3 cross section made through the same core at the same operational conditions (one flowing phase: brine, flow rate 0.1 ml/min, confining pressure 30 bar, back pressure 15 bar) before (a,c,e) and after (b, d,f) acid injection.

In order to quantify the visualisation obtained by the series of CT-scans, a fracture aperture profile over the fracture length before and after the acid injection was reconstructed in Fig. 5.4.

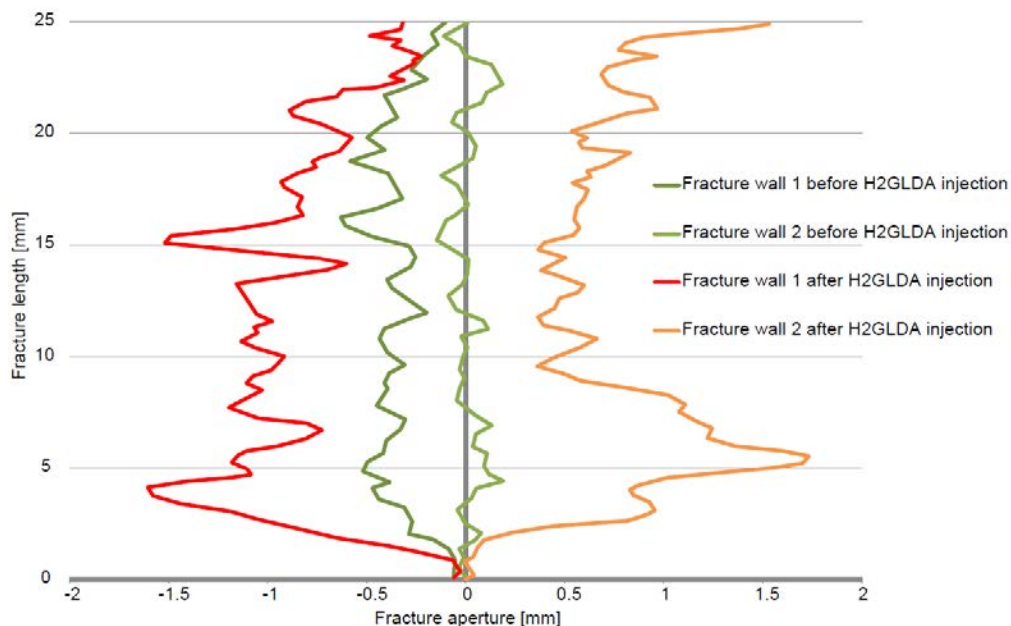


**Fig. 5.4** Fracture aperture profile over the entire fracture length before and after acid injection.

### 5.2.2 Q16-02 well sample 3 - 3837.75 – 3838.25 m

The acid injection tests were conducted on the sample obtained from well Q16-02 that contain up to 3% of carbonates. The injection of 50% diluted H2GLD (further in the text called only H2GLD) didn't result in a fracture aperture increase and in a permeability increase but in fracture closure. The single fracture that was in prior to the test created in the sample got partly cemented while injecting brine. In the formation, from where the samples were obtained, a presence of anhydrite is recognized. Thus, the process that occurs in the sample could be a result of anhydrite exposure to the brine and production of gypsum in the fracture space. After recognition of the occurred process, the injection was continued until pressure stabilization. When stable conditions were obtained, injection was switched from brine to H2GLD in order to investigate behavior under acidizing conditions.

Injection of 7PV of did not result in significant permeability improvement. The reason of above is not sufficient amount of carbonates exposed to the solution. For better illustration of the process, CT- scans taken before and after H2GLD are presented in figure 5.5.

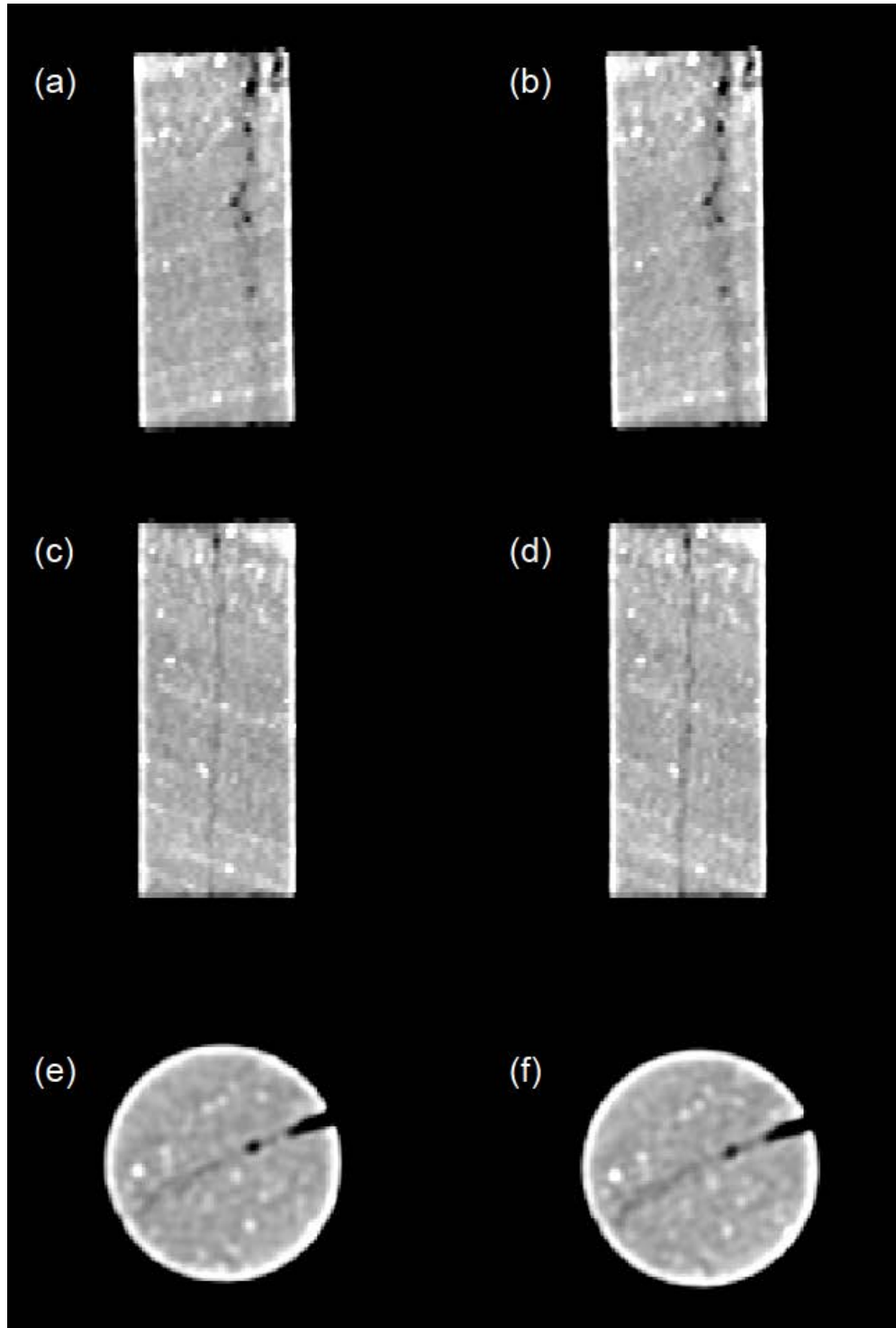


**Fig. 5.5 (a-f)** CT scans visualisation of the fracture aperture of the same core at the same operational conditions (one flowing phase: brine, flow rate 0.1 ml/min, confining pressure 30 bar, back pressure 15 bar) before (a,c,e) and after (b, d,f ) acid injection. (a,b) and (c,d) show horizontal slices, and (e,f) show cross sections at the same locations.

## 6 Conclusions

The Triassic reservoir is represented by a heterogeneous formation, with complex mineralogy, where the acid stimulation need to be planned carefully. The conducted tests confirm the TNO findings that the near-wellbore permeability can be improved. However, it strongly depends on the spatial mineral distribution and composition of the certain interval of the formation. In this study (Volpriehausen formation), the target mineral for dissolution and resulting permeability increase was carbonate. In the available samples for the intact rock studies, the volume percentage of carbonates (max 3 wt%) and its isolated accumulations were not enough to show significant changes in the flow pattern. It is possible that carbonates are not a pore throat blocking material but a pore filling material. Permeability increased over 45% in relation to the initial value, though it remained in the range of  $\mu\text{D}$ .

For the fracture studies, tests conducted on the samples that contained more than 20wt% of carbonates, showed satisfactory improvement in the conductivity of the fracture (5.4 times the starting permeability). In addition, the effect of the increased/decreased confining pressure on the permeability was not pronounced in relation to the obtained dissolution. For lower weight percentages no significant changes in permeability were observed.

It should be noted that the results of the conducted tests differ from the results reported by TNO (Rapportnummer: 0113-OEM2372.5b) due to the following: (1) The main investigated material in this report where acid injection was conducted, was from the Volpriehausen formation that was not studied petrographically; (2) The conducted tests comprise core floods in which the observed permeability alterations tend to differ from the case of dissolution tests of crashed samples.

For the numerical studies a core scale acid dissolution model was created and further matched with the experimental data by using an average value for the available reactive surface area. The obtained average available reactive surface area value from the core scale model was linked to the field scale model in order to predict the effect of calcite dissolution. The equivalent permeability was found to be a function of (1) the radius of influence and (2) the permeability improvement achieved.

The field scale simulation results showed that the acid stimulation has a positive effect on the lifetime of the reservoir. Thus, the model can be used as a predictive tool for estimating the required volume of acid injected for a certain improvement in the well productivity. It indicates the necessity of correcting the acid penetration depth (acid front) for the radial flow of acid in the formation. Thus, if the dissolution is not uniform, the penetration depth cannot be directly translated from the linear core flood data. In addition, temperature has a considerable effect on the well productivity and pump power. However, in a heterogeneous reservoir possible improvement in well productivity may not correspond to a reduction in power required by the pump.

### Recommendation

The major challenge in the geothermal energy production enhancement is the design of the fluid (acidizing) system that can improve productivity without causing incapability upon contact with formation fluids. Therefore it is recommended to undertake the number of steps:

*Sampling:* For all types of the heterogeneous reservoirs it is strongly recommended to obtain the sampling material from the reservoirs where the geothermal activities are planned. Moreover the larger quantity of samples the higher the accuracy and precision of the estimates.

#### Intact rocks

- Injection rate: To avoid damage of the formation the applied injection rate should be lower than the critical velocity. It is advised to use in the laboratory tests the planned pump rates.

## kennisagenda Aardwarmte: Soft stimulation techniques - D2

- Selection of the chemical agent: The most important is to first conduct the detail mineralogical tests, determine the cementation of the formation and further decide about the target mineral. Based on above the proper agent should be obtained and decide conduct a compatibility test with the reservoir fluids and the formation rock.

### Fractured rocks

- Injection rate: The injection rate in fractured rocks may vary from low to high and is dependent on the purpose and scale of acid penetration. A combination of different flow rates is recommended for optimal usage.
- Confining pressure application: The most important is to maintain the pressure difference between the pore and confining pressure at the level not lower than 5 bars. The most ideal is to investigate the reservoir conditions based on the well data, and further apply them to the experimental procedures.
- Selection of the chemical agent: First step is the detail knowledge about the type, geometry and composition of the fracture and filling materials. In the case of the formation damaged, history of applied operations in the well area is necessary. Secondly, the proper agent is selected based on the existing guidelines taking into consideration all possible side effects (i.e. reactions, precipitates ect) of applied fluid. And finally the dissolution tests are conducted if the material is available.

## 7 Acknowledgments

The authors would like to thank the members of the Project Advisory Group for their contribution to the development of this report. The authors thank EZ, LTO Glaskracht Nederland and het programma Kas als Energiebron for financial support of this project. The authors would like to thank also Dr. Ameri, from Akzo Nobel for providing Acid samples and his contribution to the development of this report.

## References

- Crooijmans, R. A., Willems, C. J. L., Nick, H. M., & Bruhn, D. F. (2016). The influence of facies heterogeneity on the doublet performance in low-enthalpy geothermal sedimentary reservoirs. *Geothermics*, 64, 209-219
- Saeid, S., Al-Khoury, R., Nick, H. M., & Hicks, M. A. (2015). A prototype design model for deep low-enthalpy hydrothermal systems. *Renewable Energy*, 77, 408-422.
- Matev, P. S. (2011). *Comprehensive reservoir quality assessment of Buntsandstein sandstone reservoirs in the West Netherlands Basin for geothermal applications in Zuid Holland province area* (Master's thesis, Delft University of Technology).
- Ogunjimi, O. B. (2010). *Bunter Reservoir Quality for Geothermal Applications in the Zuid Holland Area* (Master's thesis, TU Delft, Delft University of Technology).
- Brugge, J. V. M., Rutten, R. F. X., Vrouwe, B. J. (2013). *Effects of stimulation of the Main Buntsandstein geothermal reservoir in the Naaldwijk and Maasland concessions*, Rapportnummer: 0113-OEM2372.5b, T&A Survey BV (internal report).
- Nelskamp, S., & Verweij, J. M. (2012). Using basin modeling for geothermal energy exploration in the Netherlands—an example from the West Netherlands Basin and Roer Valley Graben. *Available through www.nlog.nl*.
- Fredd, C. N., & Fogler, H. S. (1999). Optimum conditions for wormhole formation in carbonate porous media: Influence of transport and reaction. *SPE Journal* 4.03: 196-205.
- Deon, F., Förster, H. J., Brehme, M., Wiegand, B., Scheytt, T., Moeck, I., ... & Putriatni, D. J. (2015). Geochemical/hydrochemical evaluation of the geothermal potential of the Lamongan volcanic field (Eastern Java, Indonesia). *Geothermal Energy*, 3(1), 1. *Deon et al. (2015)*

**Appendix 1** - Initial parameters for the homogeneous field scale modelling.

Name	Value	unit
Inlet Temperature	40	°C
Initial Reservoir Temperature	100	°C
Reservoir Depth	3000	m
Reservoir Thickness	50	m
Reservoir Length	2000	m
Reservoir Width	1000	m
Geothermal Gradient	0.03	°C/m
Pressure gradient	0.1017	Bar/m
Doublet Distance	800	m
Borehole Diameter	0.15	m
Production/Injection Rate	100	m <sup>3</sup> /s
Initial Permeability	50	mD
Initial porosity	0.1	
Injected Acid concentration	13.6	wt %
Acid injection rate	0.5	m <sup>3</sup> /min
Acid total injection time	250	hours
Acid diffusivity	1.00E-09	m <sup>2</sup> /s

**Appendix 2**

Borcore Q16-02	Interval [m]	Box top [m]	Box bottom [m]
Sample 1	Top of the box	3832.75	3833.50
Sample 2	Bottom of the box	3629.5	3630
Sample 3	Top of the box	3837.75	3838.25
Sample 4	3630.75 - 3631.33	3630	3630.75

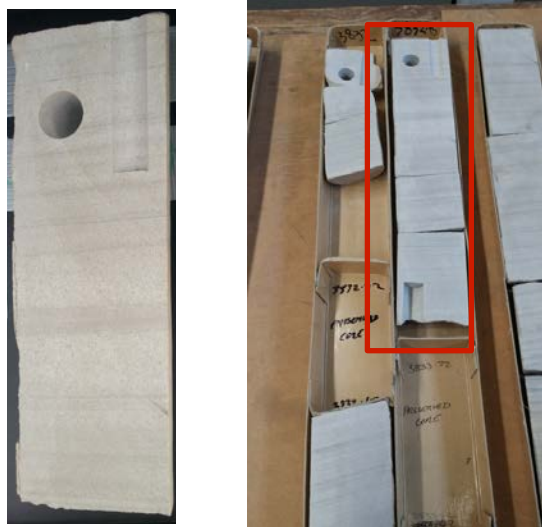


**Fig. A1.** Sample 1



Fig. A2. Sample 2



Fig. A3. Sample 3



Fig. A4. Samples 4